Chapter 10
Synthesis Methods for Carbon-Based Materials

Pradip Kumar

Abstract Carbon is a most versatile element and its bonding and special nature have long been noted largely due to the variety and quantity of structures. Carbon can make different allotropes like graphite, diamond and fullerene due to its sp^1, sp^2 and sp^3 possible hybridization nature. The development and understanding of carbon-based materials are topics of major interest in science and technology due to their excellent electrical, thermal, mechanical and optical properties. On the other hand, carbon is hardly considered to be toxic material, which makes it easily biocompatible. Carbon-based materials are synthesized using various top-down and bottom-up synthesis approaches. In this chapter, various conventional and more practical synthesis strategies, as well as their mechanism for diamond, fullerene, carbon nanotubes, carbon nanofibers, graphene and graphene oxide with the extracts from published investigations by numerous researchers, will be discussed.

Keywords Diamond · Fullerene · Carbon nanotubes · Carbon fiber · Graphene · Arc discharge · Chemical vapor deposition · Exfoliation

10.1 Introduction

Carbon-based materials like graphite, fullerene, diamond, carbon fiber, carbon nanotube, graphene, activated carbon and soot particles have been well employed for various applications due to their variety of structure and properties. For example, graphite is well-known electrode material and moderator in nuclear reactors. Graphite is mostly used in composites including in pencil, wind turbine generators, pouring nozzles, thermocouples, crucibles, etc. [1]. In addition to graphite applications, it is being used as a precursor for the synthesis of most emerging carbon materials;

P. Kumar (✉)
Integrated Approach for Design and Product Development Division, CSIR-Advanced Materials and Processes Research Institute, Hoshangabad Road, Bhopal, Madhya Pradesh 462026, India
e-mail: pradip.kg@ampri.res.in

Formely at Chemistry Division Bhabha Atomic Research Centre, Mumbai, Maharashtra 400085, India

A. K. Tyagi and R. S. Ningthoujam (eds.), *Handbook on Synthesis Strategies for Advanced Materials*, Indian Institute of Metals Series,
https://doi.org/10.1007/978-981-16-1892-5_10

graphene. Next to graphite, diamond is one of the well-known carbon materials for its hardness, high thermal conductivity, insulating and transparent properties [2]. Natural as well as synthetic, both types of diamonds are available in the market. Diamond is used in many potential applications including, optics, electronics, medical, and radiation detectors [3]. Due to their hardness, diamonds have been used for cutting, making wedding rings and other jewelry for a long time. Thus, the large-scale synthesis of diamonds with the desired size and shape is important. Another exciting form of carbon, fullerene, was discovered in 1985 at Rice University [4]. Fullerene invention won the Chemistry Novel prize in 1996. Now fullerenes have been greatly considered well-known carbon allotropes, which had previously been limited to graphite, diamond and amorphous carbon.

After the fullerene discovery, carbon nanotubes (CNTs) were first time identified in 1991 by Iijima et al. [5]. They found this new form of carbon materials during the synthesis of fullerene by an arc evaporation method. CNT is rolled from of single-layer carbon atoms. This new form of carbon-based materials has opened many opportunities for materials scientists in many fields. CNTs diameter may vary up to a few nm, while the length may be achieved in tens of micometers [6]. The most important properties of CNTs, which make them ultimate materials, are high electron mobility, thermal conductivity and mechanical strength. CNTs conducting properties highly depend on the way it constructs like armchair (metallic), zigzag or chiral (semiconductor). The ultimate properties of CNTs have been employed in many potential applications including supercapacitors, fuel cells, hydrogen energy storage, electromagnetic interference, sensors, etc. [7]. Along with, CNTs research, carbon nanofibers were also explored [8].

The major breakthrough in carbon-based materials was achieved by the identification of sp^2 hybridized single layer of carbon atoms; graphene in 2004 by Andrew Geim and Novoselov at Manchester University UK [9]. For this wonder material, they have been awarded a Physics Nobel Prize in 2010. Graphene was identified by a simple Scotch-tape method. This method produced very high-quality graphene. Graphene's unique properties like ultrahigh electron mobility, high surface area (~2600 m^2g^{-1}), large aspect ratios, the extreme thermal conductivity of ~5000 W/mK, excellent mechanical stiffness (Young's modulus of 1 TPa) and optical properties make it emerging materials for high-speed electronics, optical devices, energy storage, chemical sensors, thermal management and electromagnetic interference shielding applications [10–13]. Since graphene discovery, it has been considered a wonder material among the scientific community. Thus, the synthesis of graphene and its large-scale production is important. Many top-down including exfoliation and bottom-up including chemical vapor deposition (CVD) approaches are being used for the synthesis of graphene and other carbon materials [14–16]. In this chapter, various synthesis mechanisms for graphite, diamond, CNTs, CNFs and graphene are discussed.

10.2 Synthesis of Graphite

Graphite is one of the most stable and natural crystalline forms of carbon. It is composed of stacked layers of sp^2-hybridized carbon atoms. These stacked layers in graphite are weakly attached by weak Van der Waals force and $\pi-\pi^*$ interaction which gives its low hardness and perfect cleavage. Natural graphite can be formed by the reaction of carbon compounds in the rock during hydrothermal metamorphism. A small amount of graphite can be found in metamorphic and igneous rocks. Most of the graphite seen at earth's surface was formed at convergent plate boundaries where organic-rich limestones and shales were subjected to the pressure and heat of regional metamorphism. This process produced tiny crystals and flakes of graphite. However, synthetic graphite is required for industrial applications.

The first synthetic graphite was manufactured in the late 1800s by Edward Goodrich Acheson. He discovered it accidentally while attempting the manufacture of silicon carbide in an electric furnace. He used a combination of silica and amorphous carbon and found that silicon vaporized at about 4150 °C leaving the carbon behind in graphitic carbon. This discovery of graphite was extremely valuable and used for many potential applications. The commercial production of graphite was started in 1897 when Acheson formed a company in 1899. The synthesized graphite was found to have a purity of over 99% carbon and it is being used in manufacturing products where extremely pure material is required. Currently, many precursor materials are being used for synthetic graphite production. For example, in the USA, high-quality graphite is prepared by using petroleum coke as the primary material. Generally, the process of synthetic graphite manufacturing consists of powder preparation, shape-forming, baking and graphitization [17]. Graphite is also synthesized by the reaction of calcite with hydrogen at different temperatures, pressure and time. The synthetic graphite can be formed in various shapes and size, powders and granular materials.

Since its discovery, graphite has been employed in many industrial applications. The well-known application of graphite is in making pencils, which consist of a mixture of clay and microcrystalline graphite [1]. High purity graphite is being used for manufacturing carbon brushes for electrical motors. Composites of graphite (e.g., silver-graphite and copper-graphite) are used in wind turbine generators, railway technology and tacho generators. Composites of alumina-carbon are used in ladles for pouring nozzles, liquid steel and sliding gates. Thermocouples, heater tubes and crucible for heating are made of composites of clay-graphite and silicon carbide-graphite. Graphite is also used as electrode materials, e.g., in electric arc furnaces. Sliding bearings are made from bronze-graphite composites. Graphite powder is also used for making graphite foil which is used for manufacturing high temperature gaskets and packages. Lithium-ion and zinc-carbon batteries used high purity graphite powder as cathodic material. Graphite is also used in nuclear reactors as a moderator [18]. Not only industrial applications, now graphite is the main source for the top-down synthesis of other carbon materials like CNTs, graphene, graphene

oxide and graphene nanoribbons, which will be discussed later in this chapter [19, 20].

10.3 Synthesis of Diamond

Diamond is a second naturally occurring allotrope of carbon. The name "Diamond" is derived from the ancient Greek–adámas meaning "unbreakable". In diamond, each carbon atom is sp^3-hybridized, arranged in a variation of the face-centered cubic crystal structure. This arrangement of carbon atoms makes the diamond very hard material. Diamond has been considered one of the best materials in the scientific community as well as commercial level due to its remarkable properties including electrically insulation, high thermal conductivity, lowest thermal expansion coefficient, chemical inertness and optical transparency. Most of the natural diamond's formation occurred at high pressure and temperature in the Earth's mantle at depths of 140–190 km Natural diamond is colorless but the color in a diamond can be originated by a small number of defects or impurities such as boron and nitrogen.

Synthetic diamond has been much attracted since its establishment as a crystalline form of carbon. Initially, the diamond was synthesized using a high pressure approach due to its highest density. The first synthesis of a diamond at high pressure was developed by "General Electrics" in 1955 [21]. The Bulk amount of diamonds can be synthesized in a thermodynamic stable region at high pressure and high temperature (HPHT). In contrast, metastable thermodynamic regions at low pressure and low-temperature methods can produce thin diamond coatings and powders. To date, various methods have been successfully developed for diamond synthesis including HPHT, chemical vapor deposition (CVD), thermal activation of graphite, hydrothermal synthesis and the reduction of carbides (HSRC) [22, 23]. However, CVD is the most studied method for diamond fabrication [24]. This section summarizes diamonds synthesis by using various synthetic routes.

10.3.1 High Pressure and High Temperature (HPHT)

By using this technique, gem-purity large diamond crystals can be grown up to several millimeters. This is a conventional and effective method used for diamond synthesis for research as well as commercial applications. The HPHT method can produce high-quality sheets shape large cubic diamonds, which are mostly used for the development of cutting and grinding tools. Nevertheless, these diamonds have disadvantages such as higher cost and size limit. Many companies and researchers are using a reaction cell in HPHT conditions for the synthesis of various types of diamond crystals for commercial applications. Although they used different designs for diamond growth, typical pressure and temperatures used in HPHT are 5–7 GPa and 1200–1800 °C, respectively [25]. Generally, in the growth process, diamond morphology changes

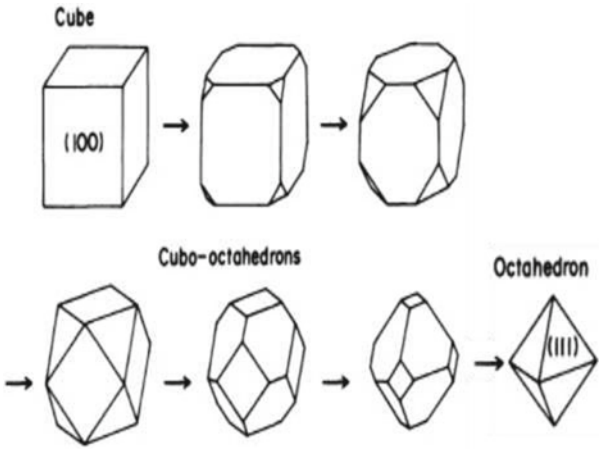

Fig. 10.1 Polyhedral of a diamond (Reproduced with permissions [25]. Copyright 1988, American Physical Society)

from cubic crystal with (100) dominated faces and cuboctahedral crystal with (100) and (111) dominated faces, to octahedral crystals with (111) dominated crystal faces with the increase of reaction temperature (Fig. 10.1).

The obtained results and method proved that they were not good enough to synthesize diamonds in that early experiment. After that many researchers modified the experimental conditions and reported good results using the HPHT method. In the modified HPHT method, Pt-30% Rh/Pt-6% Rh thermocouple was used for temperature monitoring. Room temperature pressure calibration was done by changing the resistance of standard substances. But, high temperature pressure calibration was performed by the graphite-diamond equilibrium. Liu and co-workers used carbonyl iron powder as a catalyst for diamond crystallization in the range of 5–7 GPa pressure and 1200–1800 °C temperatures [26]. A high purity graphite rod was used as source material. In this growth process, the purpose of using carbonyl iron powders was to see the effect of nitrogen and oxygen on diamond growth. The diamond growth process was performed on the mixture of graphite rod and catalyst powders (7:3, weight ratio) for 4 h. After crystallization experiments, sample columns were first cracked. The remaining impurities of graphite and catalysis were removed by dissolving the products in a hot mixture of H_2SO_4 and HNO_3. Diamond growth was first confirmed by XRD measurements as shown in Fig. 10.2. From the XRD pattern, it is evident that the sample has a cubic diamond structure which is composed of {111}, {220} and {311} characteristic lines. In contrast, the SEM image showed an irregularly shaped diamond crystal grown at 1600–1650 °C temperature without a clear {100} or {111} crystal faces (Fig. 10.3a). Further, an increase in reaction time for 15 min, diamond crystals of 0.5–0.9 mm with lamellar and strip shapes were formed (Fig. 10.3b, c). With the further increase in temperature, it was found that {111} faces played a key role in the crystallization of diamond. Diamond crystals obtained at 1700–1750 °C

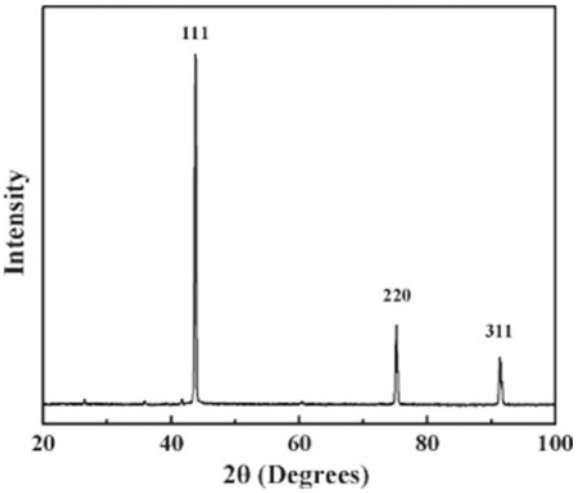

Fig. 10.2 XRD pattern of diamond crystal grown at 6.5 GPa and 1600 °C (Reproduced with permissions [26]. Copyright 2011, American Chemical Society)

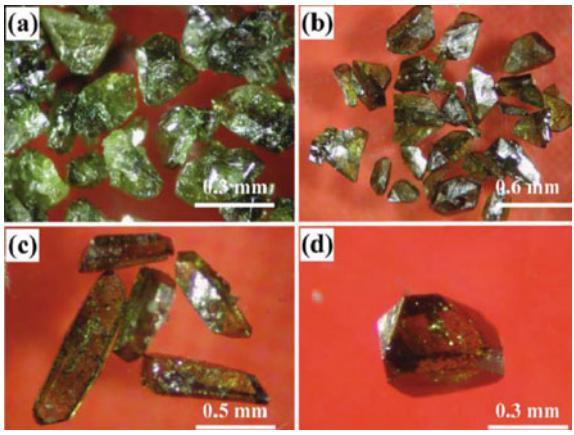

Fig. 10.3 Representative optical images of diamond crystals grown at 6.5 GPa pressure and three different temperatures: **a** 1600 °C, **b**, **c** 1700 °C and **d** 1800 °C in the presence of carbonyl iron powders catalyst (Reproduced with permissions [26]. Copyright 2011, American Chemical Society)

temperature showed {111} dominant faces and minor {100} faces (Fig. 10.3d). The above experimental outcomes revealed that high temperature conditions are more suitable for the stable growth of octahedron diamond crystals.

Diamond crystals were further synthesized from the sulfur-carbon (S–C) mixture at high temperatures (1550–2000 °C) and pressures (6.3–7.5 GPa) [27]. Graphite rod (99.99% pure), sulfur powder and cuboctahedral synthetic diamond crystals of 500 μm size as seed particles were taken as starting materials. For the nucleation of diamond crystals, first, the graphite rod was placed into a capsule of 7.2 mm diameter and 7 mm high. Then, diamond seed crystals and sulfur powder together were placed into a cylindrical sample and then placed into the graphite capsule. Then, diamond crystal growth was investigated at different temperatures and pressures for the time of 3–40 h. Growth of diamond crystals in the above system exhibited

significant dependency on temperature, pressure and nucleation time. For example, there was no diamond growth on seed crystal was found at 6.3 GPa pressure and 1550 °C temperature. In contrast, metastable graphite and slight diamond growth on the {100} and {111} faces of the seed crystals were obtained on higher temperatures (1650 °C). Even at this temperature, there was no spontaneous diamond nucleation was established. Spontaneous nucleated diamond crystals were formed at a high temperature of 1750 °C (Fig. 10.4). The size of nucleated diamond crystals was found to be ~50 μm with {111} dominant and {100} minor faces. The different surface morphology of diamond crystals was depending on the surface indices of seed crystals. For example, the flat growth of layers was found on {111} faces, while {100} and {110} faces result in pyramidal relief and striation structure, respectively. The above findings conclude that the seed crystals can form a stable octahedron diamond crystal at high temperatures. Also, metastable graphite of ~100 μm size was grown in the upper part of the capsule. Further experiment showed the regrown metastable graphite and diamond growth layers at relatively low temperatures (1550 and 1600 °C) and higher pressure (7.0 GPa). There was no sign of spontaneous nucleation of the diamond up to 40 h run. In contrast, intense diamond crystallization

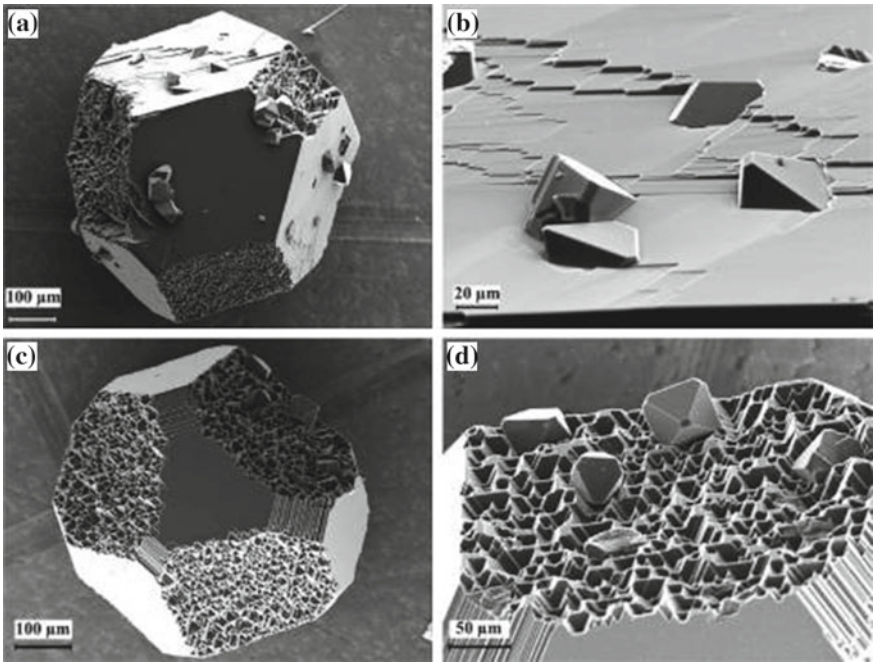

Fig. 10.4 SEM image of an overall view of diamond seed crystals, **a** spontaneous crystals and growth layers on the (111), **b** diamond seed crystal, **c** grown diamond layers on the (100) and (110) surfaces, **d** crystalline diamond obtained from 6.3 GPa pressure and 1750 °C temperature for a reaction time of 9 h (Reproduced with permissions [27]. Copyright 2009, American Chemical Society)

with more than 50% graphite to diamond conversion was found at the temperature of 1700 °C. Obtained diamond crystals show size up to 500–700 μm which can be further grown up to ~1 mm. Spontaneous nucleation of seed crystals and growth of diamond crystals were established at higher temperatures (1750, 1800 and 1900 °C) without any metastable graphite. Further, a rise in temperature up to 2000 °C gives diamond crystals of 400 μm along with metastable graphite crystals.

In recent work, Ge doped single-crystal diamond was synthesized from an Mg-Ge-C system at high pressure of 7.0 GPa and a high temperature of 1500–1900 °C [28]. The mixed powders of $Mg_{0.9}Ge_{0.1}$ and several seed crystals were used. This HPHT system produced relatively large size diamond crystals of 2–3 mm at 1900 °C. Further, they also synthesized diamond crystals using a phosphorous-carbon system at 6.3–7.5 GPa pressure and 1400–1850 °C temperature [29]. Hu et al. also developed high-quality cubic diamond crystals for commercial purposes by using a multiseed method [30]. The diamond crystals were synthesized using Fe–Ni alloy-carbon system under HPHT conditions by a temperature gradient method. Graphite powder as a carbon source and Fe–Ni alloy (64:36 by wt%) as catalyst/solvent were used, respectively. The growth temperature and pressure were set to 1250–1350 °C and 5.5–5.7 GPa, respectively. Pure and large size diamond crystals were successfully synthesized using this HPHT. But this method is extremely expensive for bulk production.

10.3.2 Chemical Vapor Deposition

The chemical vapor deposition (CVD) method is one of the most common synthesis techniques for all types of carbon-based materials. This method involves the decomposition of hydrocarbon gases and then deposition onto a substrate. In this process, a process gas, excitation source and a substrate on which sample will be deposited are required. Various gases including hydrogen, oxygen, methane, carbon dioxide, argon and nitrogen were used as process gas. To activate the chemical process, various energy sources including microwave, radiofrequency, direct current, hot filament, laser-induced and chemical activation have been used. In most of the cases, hydrogen and methane gas mixture were used for carbon-based materials. Methane or other hydrocarbons act as a carbon source, while the role of atomic hydrogen or oxygen is the most critical. The key role of hydrogen or oxygen in the CVD method is to terminate the dangling carbon bonds on the surface of the developed crystalline carbon materials. It is also reported that hydrogen atoms can cleave neutral hydrocarbons and create reactive radicals such as CH_2. The cleaved hydrocarbon can bond with exposed carbon atoms to form tetrahedral sp^3 (ta-C) or trigonal sp^2 (a-C) bonded carbon [31]. Another benefit of using hydrogen in diamond synthesis is to avoid the growth of graphite because atomic hydrogen can etch sp^2 bonded graphite much faster than an sp^3 bonded diamond.

For the first time, Eversole reported the gas-phase synthesis of diamond in 1958 [32]. This method uses a carbon-containing gas, which is passed to diamond seed crystals at a pressure of a few torr and temperature of ~1000 °C. Interestingly, it

was observed that the diamond was grown when source gas has a methyl group (CH_3–) like methane, ethane, methyl mercaptane, propane, methyl chloride and acetone. However, the low growth rate of diamond crystals of ~1 Å/h was the major issue for applications of diamond in real life. In contrast, hydrocarbon gases like benzene, which do not have methyl groups, could not grow diamonds by this method. The systematic procedure of diamond synthesis from the CVD method is illustrated in Fig. 10.5. A few years later, Angus et al. [33] also reported diamond synthesis using the CVD method on diamond seeds crystals by using mixtures of hydrocarbons and hydrocarbon–hydrogen gases. So far, the diamond has been synthesized using various modified CVD methods (Fig. 10.5b). It has been noted that diamond growth in CVD depends on various parameters such as pre-treatment of the sample, range of temperature, type of activation source and substrate selection, which play an important role. Generally, molybdenum, tungsten carbide and silicon nitride are being used as a substrate in CVD growth. In the CVD method, the temperature distribution, internal energy and solubility clearly depend on the excitation source. Based on the excitation sources, CVD processes can be divided into heated gas and ionization plasma CVD techniques which can be further sub-divided into chemical, electrical, or electromagnetically and thermal activation processes.

In the thermal activation CVD process, the gas phase is activated by hot filaments or hot surfaces as shown in Fig. 10.6 [24]. In this approach, the first process gas flows into the chamber and then hot filament was used for heating. The distance between substrate and filament can vary from 5 to 20 mm and substrate temperature can be achieved around 1000 K [24, 34]. Eiichi and co-workers reported the diamond growth by an advanced hot filament CVD method. In this method, the substrate temperature is independently controlled [35]. A mixture of CH_4/H_2 gas was used as a source precursor and silicon as a substrate. The distance between substrate and filament was maintained to 6–10 mm. Filament temperature was measured to be ~2050 ± 10 °C by an optical pyrometer. The controlled pressure of 30 torr was applied by the MKS pressure control system. The gas flow rate was maintained to ~600 sccm and the ratio of methane to hydrogen gas was 1%. It was found that diamond growth mainly

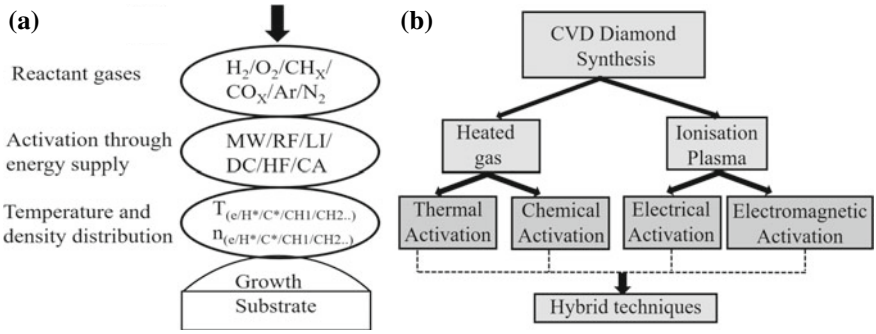

Fig. 10.5 **a** Proposed mechanism of diamond growth processes by a CVD method, **b** diamond CVD techniques (Reproduced with permissions [24]. Copyright 2011, Elsevier)

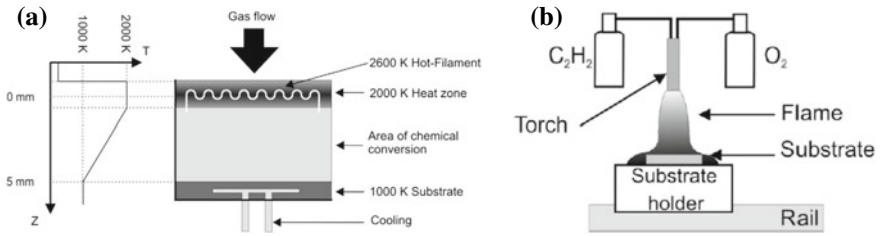

Fig. 10.6 Schematic representation of a hot filament **a** and chemical activated **b** CVD process (Reproduced with permissions [24]. Copyright 2011, Elsevier)

depends on substrate distance and its temperature. Maximum diamond growth was observed in the range of 900–1000 °C temperature. However, with the increase of substrate temperature, the growth rate was reduced. In the same year, Park et al. produced a synthetic diamond film using a hot filament CVD method [36]. They deposited diamond films on a polycrystalline titanium substrate. Direct radiation from filament was used to heat the substrate. The flow of reactant gases (CH_4 and H_2) into the reactor was controlled through a mass flowmeter. Their experimental findings revealed that surface morphology played a significant role in the nucleation and therefore in diamond film growth. The surface roughness increased the nucleation density of diamond and reduced the incubation time required for nucleation. As a result, the growth rate of individual diamond particles decreased. Further, Kobayashi and co-workers established a relationship between growth rate and flow time of source gases in the hot filament method [37]. They set the temperature of filament and substrate to 850 °C and 2100 °C, respectively. The pressure was varied from 5 to 106 kPa. In the pressure range of 5–50 kPa, all growth rates increased very fast and get maximum at a residence time of 1.1 ms. After that growth rate was abruptly deceased and saturated with residence time. Simultaneously, diamond and nanostructured graphite thin films were grown by hot filament CVD [38]. By changing the distance between substrate and filament, diamond and graphite growth can be established. At a distance of 5 mm, the diamond was obtained, while graphite deposition was observed at a distance of 15 mm.

Chemically activated growth of diamond using CVD on combustion flame was the first time described by Hirose et al. [39]. The temperature of the combusting flame can be reached in the range of 2000 to 3550 K. In chemically activated CVD processes, the heating was done by an exothermic conversion of the source gases. In general, acetylene and oxygen gases were applied for the combustion process. Generally, the substrate temperature was used from 770 to 1470 K. Figure 10.6b shows the typical setup for the combustion flame-based CVD method. The flame was generated by a commercially available oxyacetylene torch, which is vertically placed to the substrate. The whole process was controlled by changing the ratio of C_2H_2/O_2 with continuous monitoring of the substrate temperature by thermocouples and finally, diamond crystals were successfully deposited on the substrate. To increase

the deposition area, multiple torches can be used. However, chemically induced diamond deposition is not a significant method for industrial applications.

Similar to the thermally and chemically activated CVD process, diamond growth also has been demonstrated by using mixed-gas plasma [40, 41]. The common growth process in microwave plasma CVD involves placing a substrate in a quartz tube which is perpendicular to the waveguide. Microwave plasma can be generated by a magnetron. The substrate can be fully exposed to the plasma by adjusting through a plunger. Typical gas pressure was adjusted to ~40 torr and the gas flow rate was set to 10–100 sccm. The successful synthesis of high-quality diamonds using plasma CVD was developed by Setaka and co-workers. However, this method has some limitations like large-area deposition because the plasma was limited to the quartz tube size. In this context, Hiroshi et al. developed a new type of microwave plasma deposition system in which they used a high magnetic field with improved plasma density [42]. In another work, a high-quality diamond was grown from microwave plasma CVD by using graphite as the carbon source [43]. In this work, carbon is etched from graphite and placed inside the plasma. They used a conventional bell jar system for plasma generation. The hydrogen flow was fixed around 300 sccm, growth time of 24 h and microwave power was around 940 W. Silicon was used as a substrate. Diamond was grown on four different hydrogen gas pressure of 80, 100, 120 and 140 torr. At low pressure, the growth was not uniform. However, the best quality diamond was obtained at 140 torr pressure. Further, it has also been reported that diamond can be grown using a pre-treated mixed-gas-system of carbon dioxide and hydrogen [44]. However, diamond synthesized in the above methods is not feasible for industrial applications in which large-area diamond films are required.

Scalable fabrication of large-area diamonds was considered as a key step for industrial applications. Tiwari et al. reported that enhanced nucleation and diamond growth by using a microwave plasma CVD method [45]. They have grown diamond film on $Pt/SiO_2/Si$ substrate. In the deposition process, first, the substrate was cleaned by ultrasonication in acetone and alcohol for 10 min. After that, adamantine was seeded on the cleaned substrate by using ultrasonication. Diamond was grown using 1% CH_4 in H_2. The obtained thickness of the diamond film was about 900 nm for the deposition time of 120 min. However, further, the improvement was required for industrial production. Qi and co-workers reported a large area of single-crystal diamond using the microwave plasma CVD method [46]. The bulk production of diamond was achieved using 75 kW and 915 MHz microwave plasma-assisted CVD system. A mixture of $H_2/CH_4/N_2$ gases and pressures from 90 and 180 torr was used with recorded growth rates from 10 to 30 μm/h. A single-crystal diamond of 2.5 mm thickness was obtained in a single deposition run (Fig. 10.7). By using this technique, single-crystal diamonds production was achieved to 100 g/day and out of the 25% of the diamond, crystals were observed to be colorless.

Fig. 10.7 Single-crystal diamond obtained by the 915 MHz microwave plasma CVD. The diamond crystal's weights were ranged from 0.2 to 1.15 carats (Reproduced with permissions [46]. Copyright 2014, American Chemical Society)

10.3.3 Other Methods

Thermally activated graphite also can be used for diamond growth at low pressures. Palnichenko et al. reported diamond nucleation and growth using a short and intense heat pulse [47]. The diamond growth was obtained on different substrates including nickel, copper, aluminum, silicon and quartz. All the substrates were in the form of 10 cm^2 area plates and placed at a distance of 5 ± 1 mm from the electrode tip. The substrate temperature was maintained up to 10 K. As a result, well-shaped colorless diamond particles of 10 μm size were observed on the substrate as shown in Fig. 10.8. The maximum size of diamond particles can be reached up to 100 μm. The average density of diamond particles obtained by a single pulse was measured to be 10 ± 5 microparticles cm^2 with homogenously distributed irrespective of the nature of the substrate. The diamond formation was characterized using XRD, Raman and IR spectroscopic techniques.

Another alternative route for diamond fabrication is hydrothermal synthesis. Syzmanski and co-workers reported diamond synthesis by a hydrothermal process at different supercritical-fluid systems [48]. Gogotsi et al. reported diamond crystals synthesis using hydrothermal synthesis [22]. The sp^3 bonded carbon was obtained in the temperature range of 300–800 °C and pressure within 500 MPa under hydrothermal conditions by selective leaching of silicon carbide (SiC). The formation of diamond upon hydrothermal treatment of SiC has been reported elsewhere [49]. Following the above work, few researchers successfully diamond synthesis without diamond seeds by hydrothermal process. Lou et al. synthesized diamond crystal up

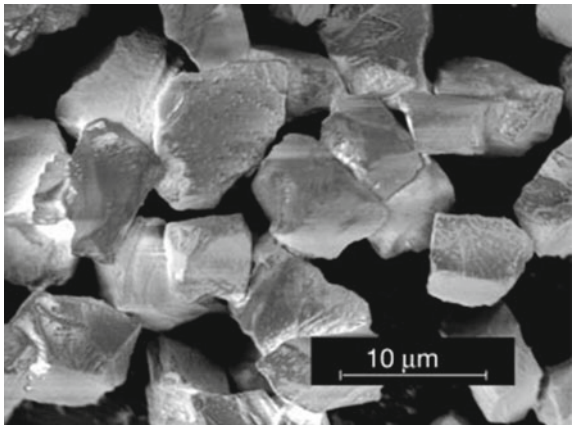

Fig. 10.8 SEM micrograph of diamond microparticles obtained by a dense carbon-phase process (Reproduced with permissions [47]. Copyright 1999, Nature Publishing Group)

to a size of 250 µm by reduction of CO_2 and magnesium carbonate with metallic supercritical- fluid sodium at a temperature of 440 °C [50].

For a long time, diamond has been popular for a variety of applications including, medicals, optics, electronics and radiation detectors. Before the graphene research, the diamond was known for the best thermal conductivity and chemical inertness [2]. Single-crystal diamonds have applications in optical science [3]. It has been well noted that pure diamond revealed the widest spectral transmission range among all solid materials. Diamond windows have been used in the chemical industry for spectroscopic quality control of molten plastics, caustic alkalies and so on. In recent years, diamond coatings have been applied to many medical devices such as temporomandibular joint prostheses, microelectromechanical systems and heart valves [51]. Functionalized nanosized diamonds have been used for the immobilization of chemotherapeutic agents. Many researchers have demonstrated imaging of cell and tissues with nanodiamond particles. Another important application of diamond is in the making of the radiation detectors. Due to its hardness, diamonds have been used for cutting, making wedding rings and other jewelry for a long time.

10.4 Synthesis of Fullerene

The first fullerene molecule was discovered by Richard Smalley, Robert Curl, James Heath, Sean O'Brien and Harold Kroto at Rice University in 1985 [4]. For this new invention, they won the Chemistry Novel prize in 1996. This new form of carbon was found to have truncated icosahedron structure and called fullerene, named Buckminsterfullerene, on the name of architect Buckminster Fuller who designed geodesic domes in the 1960s. A fullerene molecule is made from sp^2 hybridized carbon atoms. Typically, a C_{60} fullerene molecule has icosahedral symmetry closed cage structure with 20 hexagonal and 12 pentagonal rings. To date, fullerenes have

been greatly considered a well-known carbon allotrope. Since its discovery, fullerenes have been significantly considered for fundamental research as well as for potential technological applications, especially in materials science and electronics. In this section, various synthetic routes for fullerene synthesis will be discussed.

Fullerenes can be found in nature like in flames but its first experimental identification was observed in carbon vapor as shown in Fig. 10.9a. This unusual fullerene molecule was detected from laser pulse vaporized carbon species obtained from the surface of graphite, toward high-density helium flow [4]. After that vaporized carbon species traveled toward the ionization region and C_{60} can be formed at particular clustering conditions, which is about 40 times larger than the neighboring clusters. Time of flight mass spectra confirmed the most of the fullerene molecules consist of C_{60} with few C_{70} molecules (Fig. 10.9b). Figure 10.9c confirms the truncated icosahedral structure of featured C_{60} fullerene molecules. This flame technique can produce good quality fullerene molecules. However, this method produced microscopic amounts of fullerenes, which limits its commercialization.

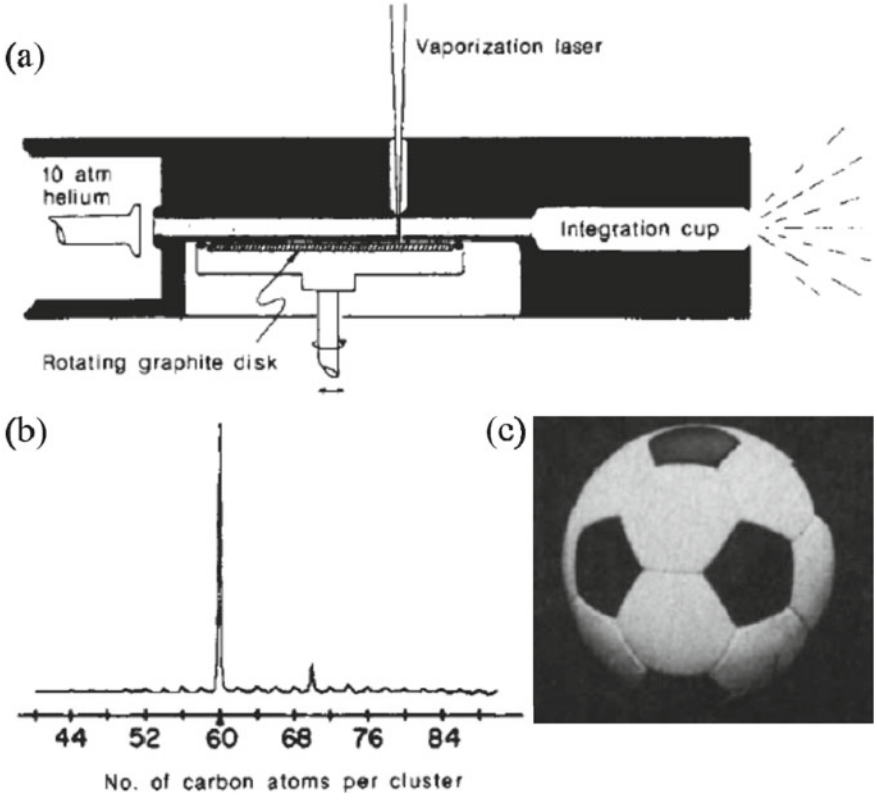

Fig. 10.9 Carbon vapor irradiation setup for fullerene synthesis, **b** time of flight mass spectra and **c** designed structure of C_{60} fullerene molecule (Reproduced with permissions [4]. Copyright 1985, Nature Publishing Group)

Since the first identification of fullerene by Kroto et al., W. Krätschmer and D. R. Huffman (K–H) synthesized C_{60} fullerene using arc method. The arc was created between graphite rods and burned under the helium atmosphere [52]. The carbon radicals were produced by slow evaporation burned graphite rod. However, the rate of clustering is slow in comparison with pulsed laser vaporization. Also, in this K-H method, the cooling rate of condensing carbon vapor is much slower. But, C_{60} clusters were successfully grown by adjusting the pressure of helium buffer gas around the evaporating graphite rods. Later, it was investigated that a simple AC or DC arc can produce C_{60} and the other fullerene molecules in sufficient quantity for commercial applications [53]. The formation of carbon clusters in the size of the range of C_{60} was easily achieved by adjusting the pressure of helium buffer gas around graphite rods. Following the above pioneering work, fullerene was synthesized using various methods like soot, vapor-phase, arc discharge, etc.

10.4.1 Soot Method

After microscopic production by Kroto et al., C_{60} fullerenes growth was identified in flames. Howard et al. reported the fullerene growth in premixed laminar flames of benzene and oxygen with Ar diluent [54]. The flame was stabilized over a copper burner of 70 mm diameter, which was used for delivering the feeding mixture. The flames were produced under various conditions. Soot was deposited for 53–170 min on quartz probe for each flame. Figure 10.10 shows the electron-mass spectrum of the as-deposited soot materials. Based on the reported data, it is confirmed that the soot

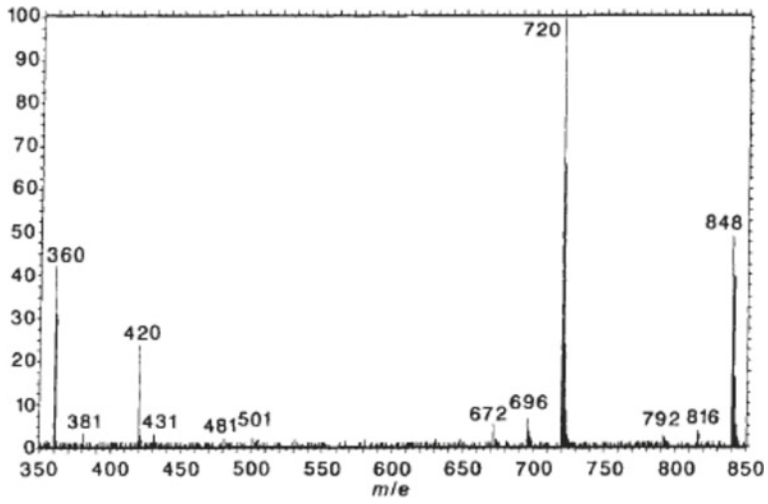

Fig. 10.10 Electron-mass spectrum of a flame-generated soot particles (Reproduced with permissions [54]. Copyright 1991, Nature Publishing Group)

sample contained both C_{70} and C_{60} fullerene molecules, which was further confirmed by FTIR.

In most of the soot method, fullerene was extracted from bulk soot [55]. The first time, Reilly and co-workers demonstrated the direct observation of fullerene growth in flame-generated soot [56]. They used a real-time measurement experimental setup for fullerene detection. They used a burner consisting of four 1.1 mm inner diameter and 1.5 mm outer diameter. A brass tube of 65 mm long was used for creating a torch-like flame. The flow rate of pure acetylene without any oxygen or air was about to be 2.4 cm^3/s through the burner tubes. Soot particles were collected onto exhaust snorkel of 4-inch diameter, which was placed over the flame. The sample tube was allowed to cool down automatically. Based on their experimental findings, it was concluded that the carbonization process of polycyclic aromatic hydrocarbons (PAHs) produced fullerene in the particle phase. This method also produced individual soot particles in low quantities. In summary, by this technique, we can track the composition of fullerene molecules.

10.4.2 Chemical Vapor Deposition

Similar to diamond growth, fullerene formation was demonstrated by CVD using gaseous species such as CH_4 or C_2H_2. Lee et al. reported the fullerene formation during the synthesis of diamond film using the CVD method [57]. The experiment was performed in a conventional hot filament CVD chamber having an 8 cm tungsten filament of 0.75 mm diameter. The current and filament temperature was maintained about 50–55 A and ~2200 °C, respectively. The pressure of the chamber was maintained from 30–35 torr. Methane (99.8% pure) and H_2 (99.99% pure) were used as precursor gases with a controlled flow rate. Silicon wafer placed on flat stainless-steel was used as a substrate and maintained at a temperature from 850 and 900 °C. Fullerene deposition was obtained between 5 to 24 h. In each run, 10–75 mg soot was collected soot. Mass spectrum measurements confirmed the fullerene growth in the hot filament CVD method. Further, it was found that changing the composition of precursor gases (2–5% CH_4, 95–98% H_2), substrate temperature (400–750 °C) and moving the substrate away from filament enhanced the growth of fullerene formation to 10–20 mg/h. There was a strong correlation between the diamond and the fullerene growth process. Figure 10.11 shows the diamond and fullerene formation by using the above process (solid arrow) and by other researchers with other routes (thin arrow).

Some other researchers have also developed other CVD methods for fullerene formation [58]. Fullerene was formed by low-temperature plasma CVD under atmospheric pressure [59]. Low-temperature plasma was generated by applying rf voltage under a constant flow of atmospheric pressure Ar or He gas. Benzene or naphthalene gases were used as a source for deposition. At He (70 sccm) and 70–100 rf powers, the gas plasma produced a tary deposit upon the flow of naphthalene or benzene (0.01–1 sccm). The products from naphthalene (0.3–0.6 sccm) formed soot when Ar

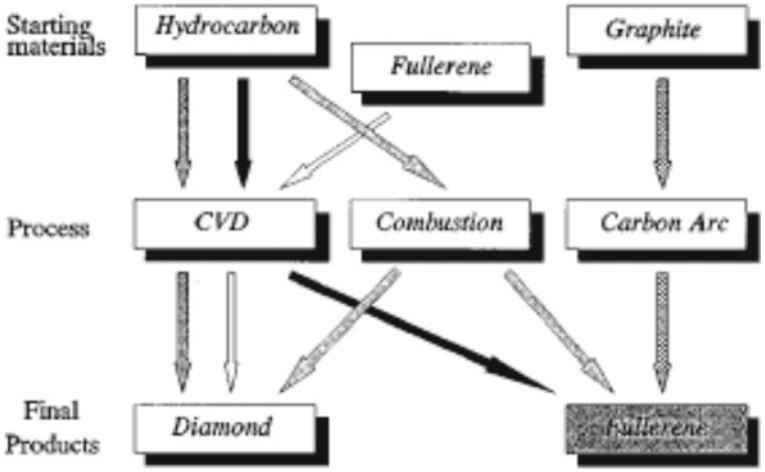

Fig. 10.11 Formation of diamond and fullerene by several processes using different starting materials (Reproduced with permissions [57]. Copyright 1995, American Institute of Physics)

(13 sccm) was introduced into He (47 sccm) plasma. It was found that product appearance depends on the plasma conditions. Fullerene formation was confirmed by UV–visible spectra. Further, Wang et al. produced the Fe-included onion-like fullerenes at a temperature of 1100 °C [60]. The diameter of the as-synthesized fullerenes was in the range of 15–40 nm which was confirmed through microscopic techniques. In this method, fullerene growth mainly depends on the substrate temperature and carbon source.

10.4.3 Arc Discharge

Since its development in the 1990s, the arc discharge method has been considered an effective and popular method for large-scale synthesis of fullerene [61, 62]. In this method, graphite electrodes are vaporized in a low pressure helium atmosphere. Arc is generated by passing the current through electrodes and fullerene containing soot was formed. Kratschmer's group in 1990 developed the first arc discharge system which is the most popular technique for fullerene synthesis till now [52]. After that several authors demonstrated fullerene formation using the arc discharge method. It was found that fullerene formation strongly depends on the operation parameters of carbon plasma-like very high temperature and inert atmosphere at reduced pressure. The typical setup of the arc discharge method is mainly composed of a stainless-steel double-walled cylindrical chamber [63]. Both graphitic electrodes were mounted horizontally near the bottom of the reaction chamber. But anode is mounted in a controlled guiding mechanical system for maintaining a constant distance between both electrodes during arc discharge. For soot formation, the chamber is evacuated

until a pressure of 10^{-3} to 10^{-4} torr. The chamber was filled with an Ar or He gases at the pressure 50–200 torr at 30 ± 2 °C during the process. From the obtained soot, C_{60} fullerene was extracted with toluene and by vacuum evaporation. Fullerene formation was confirmed by XRD measurements. The yield of fullerene synthesis was up to 6–8% which was higher than previous reports. The best yield of fullerene synthesis (~8%) was achieved at an arc current of 150 A and 100 torr of chamber pressure.

It has been noted that synthesis yield depends on the thermal and photochemical stability of C_{60}; however, both have not been defined well. The experimentally low decomposition temperature of 1000 K was determined for C_{60} in a vacuum [64]. Theoretical results showed the fullerene stability up to a temperature of 1800 K [65]. In general, C_{60} has been considered a relatively stable molecule. However, it can degrade under a variety of conditions [66]. It was demonstrated that fullerene decomposition significantly depends on the intensity of emitted light energy [67, 68]. The arc gap also influenced fullerene yields. The maximum yield was reported for large electrode gaps (2–4 mm) [69, 70]. However, in contrast, in some studies maximum yield was reported at a smaller electrode gap [71]. This contrast in experimental findings is considered due to large experimental errors [72].

The first experimentally investigation of the arc gap on the fullerene formation is reported by Andrzej et al. [53]. They optimized the experimental parameters such as input power, pressure, buffer gas and AC or DC feeding mode. The electrode gap was set to 0.5 mm with 4 mm for DC arcing. The whole system is controlled by an optoelectronic system of 0.2 mm accuracy. Initially, the electrodes were positioned close together. In contrast to the conventional method of striking anode against cathode, high-voltage glow discharge was used for arc discharge intimation. A helium pressure of 13.3 kPa was used for tests. The quantity of fullerene resulting from soot obtained from electrode arcing was tested by conventional spectrophotometric techniques. Based on their experimental observation, a significant distinction was found at a smaller electrode gap, while larger gap distance gave a significant difference in the fullerene formation. The fullerene content decreases with the increase of the electrode gap. Further, they also found that not only the electrode gap but also complex vaporization and mass transport phenomena greatly influenced the fullerene yield. Further, fullerene synthesis was also demonstrated from DC discharge between carbon electrodes in the mixture of Ar and ferrocene gas [73]. Another alternative, the solar energy-based approach was also developed for fullerene synthesis [74].

Fullerene has received much attention for a wide range of applications due to its interesting features including nonlinear optical properties and superconductivity [75]. Fullerenes have potential applications in 2D/3D metal–organic frameworks, solar energy conversion, liquid crystals materials, thermoresponsive materials and C_{60}-polymer hybrid materials, etc. [76–80]. Fullerene's unique shape and hydrophobic nature make it very effective for medical applications including sensitizers for photodynamic therapy and as photoactive molecular devices [81, 82].

10.5 Synthesis of Carbon Nanotubes

Carbon nanotubes (CNTs) have received first recognition in 1991, but their history goes long back. Radushkevich and Lukyanovich [83] first observed and described CNTs in 1952, which was later confirmed by Oberlin et al. in 1976 [84]. However, CNTs received significant research interest after its discovery in 1991 by Iijima et al. [5]. MWCNTs were obtained, while they were developing a new arc evaporation method for the synthesis of C_{60} fullerene. After two years later, Iijima et al. [85] described the growth mechanism of SWCNTs. CNTs have a tubular structure with a diameter as small as 1 nm and length can be varied from few nm to microns. The construction principle of SWNTs using a graphene sheet along the chiral vector C is shown in Fig. 10.12 [6]. CNT's structure can be zigzag, armchair, or chiral, totally depending on the chiral vector during construction, which determines its most of the properties. For example, Dresselhaus et al. investigated the electrical properties of CNTs constructed from different chiral vectors [86]. Thus, CNTs properties depend on its structure like chiral angle, length, diameter, etc., which can give them unique properties. Due to the exceptional properties of CNTs, they have been considered novel nanomaterials for a wide range of applications.

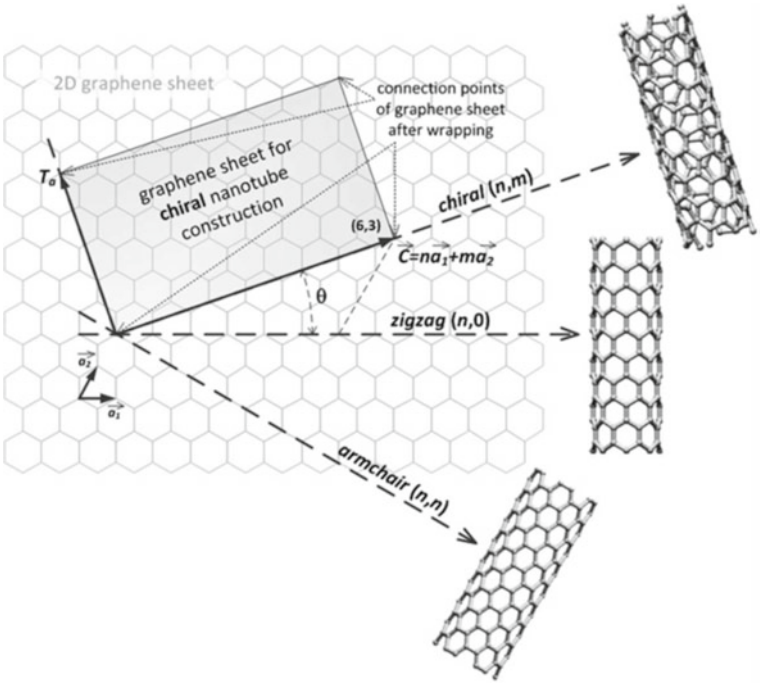

Fig. 10.12 The principle of CNTs construction using a graphene sheet (Reproduced with permissions [6]. Copyright 2011, The Royal Society of Chemistry)

For fundamental study and commercialization of CNTs in the field of material science, various synthesis methods such as CVD, laser ablation and arc discharge have been developed. CNTs were first prepared using arc discharge techniques and then followed by a low-temperature CVD technique (<800 °C). Later, other non-standard methods including liquid pyrolysis and organic approach were also developed. Irrespective of techniques, CNTs can be synthesized in the form of single-wall carbon nanotubes (SWNTs), double-wall carbon nanotubes or multi-wall carbon nanotubes depending on the experimental parameters.

10.5.1 Arc Discharge

Since its first identification by Iijima et al., CNTs growth have been developed by many other groups. The arc discharge technique produced CNTs at higher temperatures (>1700 °C). Arc discharge technique produced CNTs have shown some structural defects. Figure 10.13 showed a typical experimental setup of the arc discharge technique [87]. The arc chamber is composed of two electrodes (anode and cathode) which are mounted vertically or horizontally. The cathode is filled with a pure graphite rod and the anode is filled with powdered carbon precursor along with the catalyst. High temperature is achieved from created arc discharge. SWNTs can be produced by using graphite rods doped with metal catalysts like Fe and Co as the anode and pure graphite as a cathode [5].

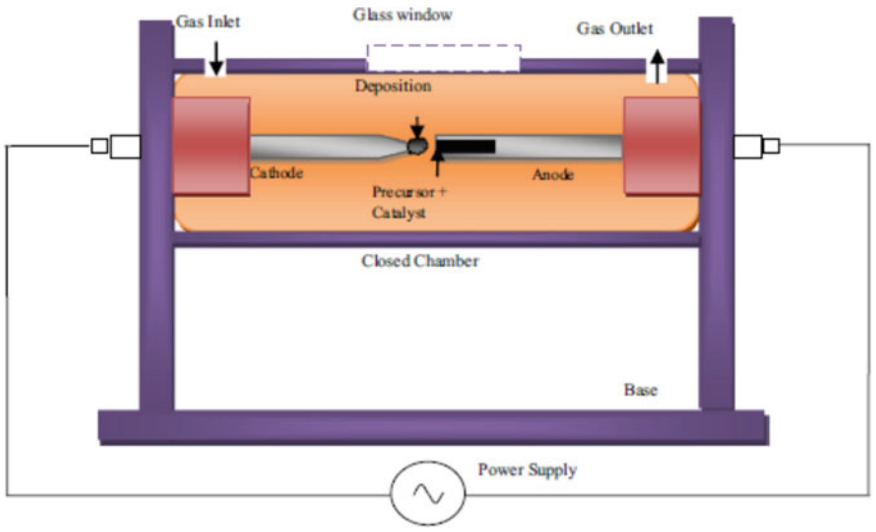

Fig. 10.13 Schematic of an arc discharge for CNTs (Reproduced with permissions [87]. Copyright 2014, Elsevier)

The synthesis of SWNTs was further reported by carbon evaporation with cobalt [6]. Nickel has been considered the most widely used catalyst for SWNTs synthesis. The catalytic role of the growth of carbon nanoclusters was investigated using dc arc discharge. Nickel-filled anode improves the growth of SWNTs [88]. SWNT's growth was further investigated with platinum-group metals (Ru, Rh, Pd, Ir, Pt) and it was found that only Rh, Pd and Pt were found to have catalytic activity for growing SWNTs of 1.3–1.7 nm diameters [89]. In another study, it was found that Mo improved the yield of soot [90]. However, the purity of SWNTs in collected soot was not changed significantly. The mass production of SWNTs can be achieved by using a bimetallic Ni-Y catalyst under He ambient gas [91].

Similar to SWNTs, double-walled nanotubes (DWNTs) were synthesized by the arc discharge method. However, DWNTs synthesis from the arc discharge method is much more complicated in comparison with SWNTs production. Many research groups reported DWNTs synthesis using the arc discharge method [92–94]. Hutchison et al. reported the production of DWNTs from the arc discharge technique by using a mixture of argon and hydrogen [94]. The obtained materials were confirmed as bundles of DWNTs along with SWNTs as a by-product. Further, high-quality DWNTs was synthesized from high temperature pulsed arc discharge method [95]. Later, Huang et al. reported the synthesis of super bundles of DWNTs in a hydrogen-free atmosphere [96]. Liu et al. synthesized selective DWNTs by hydrogen arc discharge technique with nickel formate dihydrate catalyst [97]. Graphite powders or MWNTs/carbon nanofibers were used as a carbon source (Fig. 10.14). The HRTEM results confirmed around 80% DWNTs and the rest of were SWNTs and ends of DWNTs were uncapped. In this work, it was also found that the growth of DWNTs mainly depended on the cobalt catalyst [98].

Arc discharge methods were also used for the production of MWNTs. The morphology of MWNTs depends on the synthesis conditions. Some groups have reported the use of methane or hydrogen atmosphere for MWNTs growth. Wang et al. reported MWNTs synthesis using DC arc discharge under the helium and methane atmosphere [99]. Thin and long MWNTs were obtained by using methane

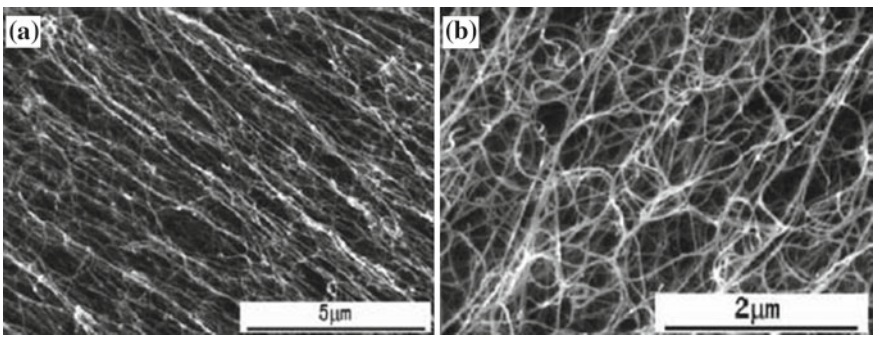

Fig. 10.14 SEM images of the as-synthesized DWNTs (Reproduced with permissions [97]. Copyright 2007, American Chemical Society)

gas pressure of 50 torr and an arc current of 20 A for the anode. Further, long and fine MWNTs can be prepared under a hydrogen gas atmosphere. But a big difference was found with the use of He and methane gas atmosphere. It was found that methane and helium gases atmosphere give more carbon smoke in comparison with the hydrogen gas atmosphere [23]. In another work, it was found that DC arc discharge in the hydrogen gas atmosphere can produce long MWNTs and graphene sheets as a by-product [24]. MWNTs were also synthesized at various pressures ranged from 150 to 500 torr under acetone, ethanol and hexane atmosphere. It was demonstrated that the production of MWNTs was at least two times higher in ethanol, acetone and hexane atmospheres than that of MWNTs produced in the He atmosphere.

Further, the growth of MWNTs was also reported from the arc discharge deposition process with the use of a pulsed laser. Parkansky and co-workers used a single-pulse arc for the synthesis of MWNTs in ambient air [100]. MWNTs were deposited vertically oriented on Ni/glass substrate with a length of up to 3 mm and a diameter of about 10 nm with a single 0.2 ms pulse. Tsai et al. also demonstrated MWNTs with an inner and outer diameter of 5 and 17 mm, respectively by using single-pulse discharge in the air [101]. Moreover, there are several reports on MWNTs deposition by using a gas atmosphere with arc discharge in liquid solutions. Sornsuwit et al. reported the synthesis of high-quality SWNTs and MWNTs in H3VO4 aqueous solution from pure graphite electrodes through arc-discharge [102]. HRTEM analysis revealed the high-quality well-ordered MWNTs without any defects. The outer diameter of MWNTs was 10–20 nm and interlayer distance of ~ 0.35 nm between graphene layers [103]. Similarly, the synthesis of MWNTs in high yield can be obtained by arc discharge in liquid nitrogen [104]. Arc discharge in water can also produce high yield MWNTs production [105].

10.5.2 Laser Ablation

Laser ablation methods have been successfully developed for the production of SWNTs and MWNTs. For the first time, the Smalley group demonstrated the principles and mechanisms of CNTs growth by laser ablation technique [106]. Generally, Nd: YAG and CO_2 lasers are being used in the laser ablation method. In this method, the graphite target is vaporized by a laser beam at high temperatures under an inert atmosphere. The laser generates carbon species, which are swept by the flowing inert gas from the high temperature zone to a conical water-cooled copper collector. The reaction temperature is an important parameter in CNTs production quality and yield. It was reported that the size and average diameter of CNTs can be tuned by tuning the laser power, growth temperature, catalyst composition, type of gases and its pressure [107–109]. Maser and co-workers demonstrated the high-density SWNTs obtained from a simple CO_2 laser system [110]. Also, it was found that laser power, the wavelength of laser and pulse duration can play a key role in the properties of the final product [111]. For example, the average diameter of SWNTs increased with

the increase of CO_2 laser power from 500 to 800 W. However, the excitation wavelength growth mechanism of CNTs has not been clearly understood. Chen et al. [112] reported that SWNTs diameter can be controlled by varying the furnace temperature, catalytic metals and flow rate. Higher furnace temperature produced SWNTs with larger diameters. It was found that the use of a Ni–Y alloy catalyst increases the SWNT diameter, whereas an Rh-Pd catalyst reduces it [113].

For commercial purposes, polystyrene-MWNTs thin films deposited on alumina substrates by PLD techniques with Nd: YAG laser ablation [114]. High-quality DWNTs and SWNTs were produced from a combined method of steady arc discharge and the laser-furnace methods [115, 116]. Impurities such as catalytic metals and amorphous carbon present in CNTs can be removed by purification processes based on chemicals such as H_2O_2 or oxidation by hot air (400–500 °C) [117]. Both arc discharge and laser ablation techniques can give high-quality growth of CNTs, but these are expensive techniques due to high power equipment. Also, the CNTs production yield is low in both methods.

10.5.3 Chemical Vapor Deposition

To date, the CVD technique has been established as one of the best methods for CNTs production. In this method, CNTs are formed by the decomposition of the carbon precursor on the catalytic substrate surface. Thermal or plasma CVD is considered as the standard method for CNTs synthesis. Also, other CVD techniques such as hot filament (HFCVD), water-assisted CVD, oxygen assisted CVD, radiofrequency CVD (RF-CVD) or microwave plasma (MPECVD) have been developed [118–121]. CVD techniques are very economical for industrial production of quite pure CNTs in comparison with laser ablation. In this technique, first, a catalyst is prepared and then the actual synthesis of nanotube was performed. The catalyst role in the CVD method is to improve the decomposition of the carbon precursor. When the catalytic substrate is heated up in a carbon-rich gaseous environment, CNTs were produced at 500 to 1000 °C. The advantage of CVD techniques over arc discharge or laser ablation is that it can produce CNTs in many forms like straight or coiled, films and vertically aligned structures.

The systematic of catalytic CVD reactor system for CNTs synthesis is shown in Fig. 10.15a [122]. A mixture of xylene-ferrocene was used as a carbon source into an inert gas medium. The reaction starts with the decomposition of the ferrocene-xylene mixtures at atmospheric pressure and temperatures of 625–775 °C. As obtained nanotubes were highly pure (Fig. 10.15b, c) with a maximum length of ~50 μm. Many substrates including Ni, Si, Cu, Cu/Ti/Si, SiO_2, etc. were used CNTs growth [123]. CNTs growth was also investigated on the mesoporous silica substrate as it can play as a template for the initial nanotube growth [124, 125].

In the CVD technique, the selection of catalysts is a very important parameter for CNTs growth. The effect of catalytic nanoparticle composition and morphology on CNTs growth in the CVD method has been demonstrated [126]. Also, CNTs

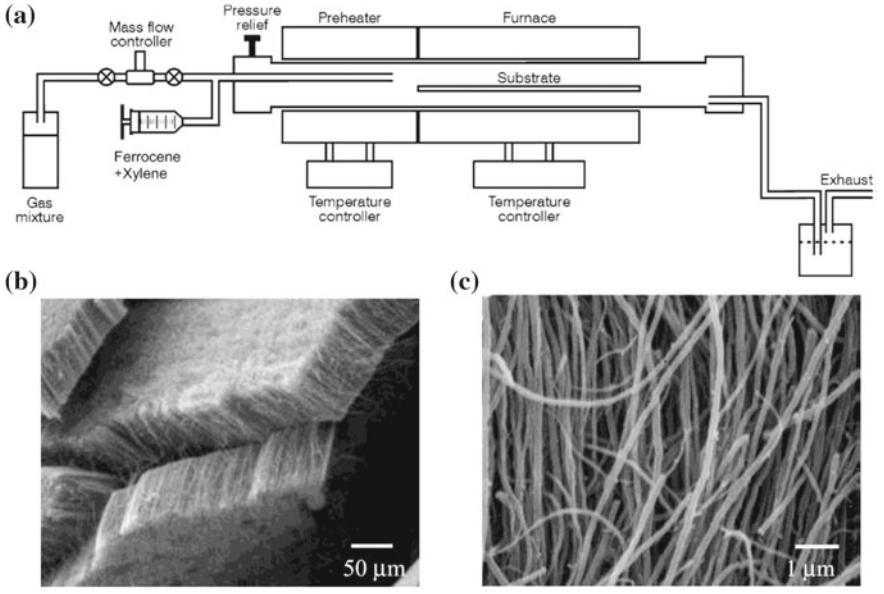

Fig. 10.15 **a** A representative scheme for the production of MWNTs using catalytic CVD reactor. **b** as grown SEM image of well-aligned MWNTs arrays and **c** higher magnified SEM image obtained from catalytic CVD method (Reproduced with permissions [122]. Copyright 2002, American Chemical Society)

growth was reported from catalysts derived from Co/Fe/Al layered double hydroxides (LDHs) [127]. It was found that Co content in precursors showed a significant effect on CNTs growth. CNTs with a smaller diameter and fewer defects were formed at higher Co content. In another work, Flahaut et al. investigated the catalytic effect on the preparation of CNTs [128]. The results showed a significant effect of catalyst composition on CNTs growth. Jiang et al. reported the in situ growth of CNTs on the pre-treated graphite electrode in the presence of $Ni(NO_3)_2$ catalyst via CCVD method. For a shorter growing time, MWNTs revealed the length of 200–1000 nm with the inner and outer diameter of 20 and 80 nm, respectively [129].

Not only catalysis, but carbon source also is a key parameter for CNTs growth. High-quality DWNTs can be obtained by decomposition of benzene at 900 °C in the presence of Fe-Mo/Al_2O_3 catalyst [130]. As-prepared DWNTs bundles were found without any amorphous carbon on the surface, with fewer structural defects. Further, the well-aligned MWNTs were obtained via pyrolysis of C_2H_2 on a large area of Ni deposited Si/SiO_2 substrate using the thermal CVD technique at 900 °C [131]. The studies showed the crucial effect of NH_3 pre-treatment on the surface morphology metal catalyst and therefore to get the vertical aligned CNTs. Highly aligned CNTs can be obtained at a higher density of Ni particles due to the effect of steric hindrance between neighboring CNTs. It was found that the degree of CNTs crystallization increased with the increase of NH_3 pre-treatment time. The

detail of the direct growth of aligned CNTs, substrate effect, growth mechanism and advantages and shortcomings of CVD have been reviewed [132]. Some researchers used Nickel oxide-silica binary aerogels as the catalyst for the growth of MWNTs by decomposition of methane at 680 °C for 120 min. The diameters of DWNTs were observed to be 40–60 nm [133]. Also, CNTs can be grown using two carbon sources of ethanol/Co and benzene/Fe systems [134].

CNTs were further grown by plasma-enhanced CVD (PECVD). The use of the PECVD method for SWCNTs has been well summarized by Lim et al. [135]. PECVD method gives high-quality CNTs. Forest like MWNTs deposited on a solid substrate is shown in Fig. 10.16. PECVD methods can be used in many different modes: direct current (DC-PECVD), radio frequency (RF-PECVD), diffusion (DPECVD) or microwave (MWPECVD). Like thermal CVD, CNTs synthesis using DPECVD has been demonstrated on the various substrate (i.e., Ag, Pt, W, Ta, Ir and NiV) at low-temperature (480–612 °C) [136]. Vollebregt et al. [137] reported self-aligned vertically grown CNTs and CNFs by using Pd as catalyst material. Samples were fabricated using a different catalyst (Pd, Ni, Fe, Co) and at different temperatures such as 450–640 °C for atmospheric pressure chemical vapor deposition (APCVD) and 450–500 °C for PECVD. APCVD produced highly dense self-aligned CNTs when Pd acts as the catalyst, while the random growth of CNTs was found in the Co and Fe catalyst. Further, they also concluded that CNTs grown by PECVD in the presence of Pd catalyst, produced large bundles of tubes, while large-diameter CNFs were formed in the presence of Ni catalyst. Biocompatible supported CNTs electrodes also have been developed using the CVD method by using ferritin as the catalyst. This type of CNTs electrodes might be useful in neuro-implants [138].

Since its discovery in 1991, CNTs have stimulated intensive research in the area of nanotechnology due to their outstanding electronic, thermal and mechanical, properties. Their implementation in various potential applications forms a great research effort and is now in progress. CNTs application has been demonstrated in scanning

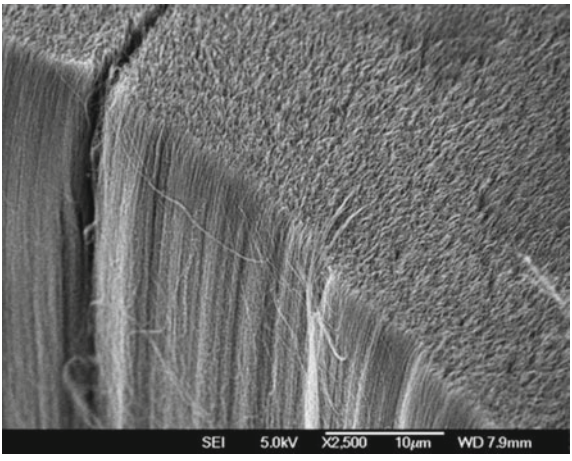

Fig. 10.16 SEM image of forest type MWNTs produced from PECVD at atmospheric pressure (Reproduced with permissions [135]. Copyright 2010, Springer)

tunneling microscopy tips. CNTs have also been demonstrated for solar cells, fuel cells, biosensor, hydrogen storage media and carbon–metal composites for strong and lightweight structures applications. In summary, low cost, rapid and readily scalable route for carbon nanotubes fabrication have been developed for all future applications.

10.6 Synthesis of Carbon Nanofibers

The first synthesis of carbon filaments was reported in the 1970s, but the significant research was carried along with the discovery of CNTs in 1991. These carbon filaments with the cylindrical structure are known to be as carbon fibers (CFs). They can be nanofibers or microfibers, depends on their diameter. Carbon nanofibers may have different microstructural configurations like platelet CNFs as shown in Fig. 10.17 [139]. Herringbone CNFs are formed when graphite sheets are inclined from the fiber axis with some angle. The next structure is tubular CNFs, wherein graphite sheets and fiber axis are parallel to each other. Based on their morphology, CFs can be produced in various shapes including planar, twisted, branched, coiled, spiral, helical and so on. Mainly chemical vapor deposition and electrospinning method have been adapted for significant synthesis of carbon fibers. However, other methods including template-assisted, hot-filament assisted sputtering and microwave-based synthesis have also been reported. In this section, the synthesis and mechanism of carbon fibers using the CVD and electrospinning method will be discussed.

10.6.1 Chemical Vapor Deposition

Again, the CVD technique has been considered as one of the most versatile approaches for carbon nanofibers synthesis. CVD techniques have been developed for scalable and reproducible synthesis of CNFs, in which gaseous precursors such as C_2H_2 and CH_4 are used on a metal catalyst support at elevated temperature. Typically,

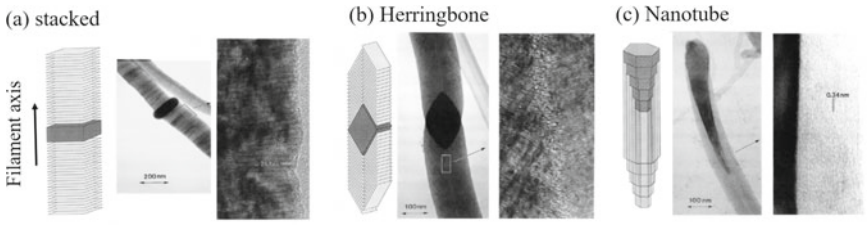

Fig. 10.17 Schematic representations of platelet (**a**), herringbone (**b**) and tubular (**c**) CNFs to the filament axis (Reproduced with permissions [139]. Copyright 1995, American Chemical Society)

the use of catalysts, the chemical composition of precursor and reaction parameters define the final structure of the product. In this method, hydrocarbon decomposition of carbon precursor provides a continuous supply of carbon to produced well-organized tubular filaments of sp^2-carbon in hexagonal form. However, this technique is expensive and also produces short fibers [140].

Catalytic thermal CVD (CTCVD) was mostly used for the fast growth of helical carbon fibers. In the early 1990s, Motojima et al. [141] first time used the CTCVD method for the synthesis of regular coiled shape carbon filaments. The CFs were synthesized by pyrolysis of acetylene on Ni-catalyzed substrate at a temperature of 350–750 °C. The obtained CFs were found to be composed of pair-coiled fibers. These fibers are elastic and can extend up to three times the original length of the coil. Figure 10.18 showed the perpendicular grown carbon coils on the graphitic substrate [142]. Catalyst Ni grain material was found on the tip of all carbon coils, which is shown by arrows. The diameter of the regular carbon coils was ~3 to 6 μm with the coil pitch of 0.5–0.7 μm without any gap. For the reaction time of 2-h, coil length was increased up to 5–8 mm with a growth rate of 7 μm/s. The high yield of carbon nanocoils was obtained by using acetylene as a carbon source and iron-coated indium tin oxide as catalytic material [143]. Similar to CNTs synthesis, CF synthesis has been developed by the decomposition of acetylene, methane, ethylene, etc. over various transition metals catalysts including Fe, Co, Ni, etc. in the temperature range of 500–1000 °C [144, 145].

Further, carbon nanocoils (CNC) were produced by the low-temperature decomposition of acetylene [131]. The obtained CNCs exhibited a yield of 11 g in each run and formed a nanospring. Minea et al. [146] prepared carbon nanofibers at room temperature by plasma-enhanced CVD. They used low pressure, high-density plasma technique and grown the fibers on a thick Ni film deposited upon a silicon substrate. The CNFs were scratched from the substrate by a diamond tip. The obtained CNFs

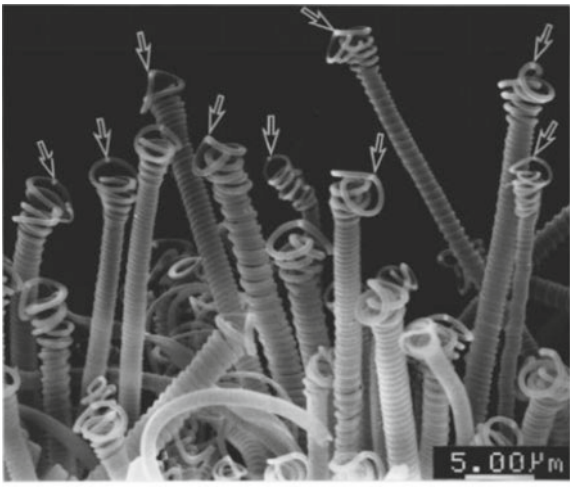

Fig. 10.18 SEM image of vertically grown carbon coils on the substrate (Reproduced with permissions [142]. Copyright 1999, American Institute of Physics)

were amorphous and have a short length of ~50 nm at a deposition rate of 2 nm/min. Carbon nanofibers are also synthesized without any catalyst by microwave pyrolysis CVD using N_2 as a carrier gas and CH_4 as a source at a temperature of 1050–1150 °C [147]. Carbon fibers are radially grown on the porous Al_2O_3 substrate. The prepared CFs were uniform in diameter in the same region. Simultaneously, it was also noted that the ends of fiber were hemispheroidal and some cauliflower-like fiber ends can also be observed in the as-prepared samples.

10.6.2 Electrospinning

Commercial synthesis of carbon fibers was obtained from the electrospinning method. The first patent on electrospinning was published by Cooley in 1902. After that, researchers produced carbon fibers through electrospinning [148]. However, this method got much attention in the last two decades and is optimized for carbon fibers fabrication. This technique is based on the processing of polymeric solutions or melts by using an electrically force fluid system [149]. In the electrospinning process, there are many controlling parameters such as solution properties and processing parameters as well as on surrounding temperature and humidity conditions [150]. The structure of CNFs strongly depends on the nature of the polymeric precursor. The CNFs fabrication has been reported using various polymeric precursor including polyacrylonitrile (PAN), pitch, cellulose, poly (amic acid) (PAA), polybenzimidazole (PBI), polyimide (PI), poly (p-xylenetetrahydrothiophenium chloride) (PXTC) and poly (vinyl alcohol) (PVA) [151, 152]. High-quality CNFs production can be obtained by selecting the right organic polymers, followed by thermal annealing under inert conditions.

Kong et al. [153] successfully synthesized CNFs by electrospinning of PAN/DMF polymer solution and then stabilization and carbonization. The stabilization was carried out in the air between temperature 200 to 300°C. The carbonization process was performed at 2800°C under an inert atmosphere (Fig. 10.19) [154–157]. CNFs

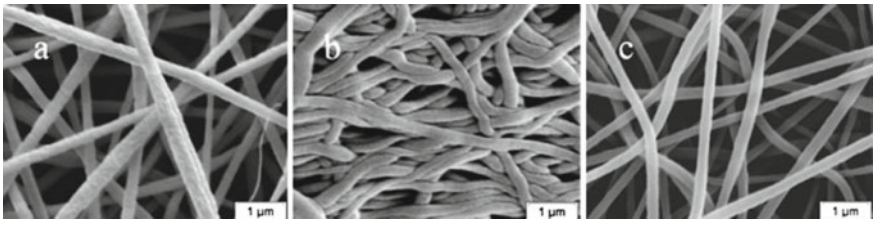

Fig. 10.19 **a** Typical SEM micrograph of electrospun PAN nanofibers obtained from 8% PAN solution in DMF, **b** CNFs produced from a two-step heating: 200 °C for 30 min and 750 °C for 1 h and **c** CNFs produced from a multi-step progressive heating: 5 °C/min from 30 to 230 °C, 1 °C/min from 230 to 270 °C, then 5 °C/min from 270 to 800 °C (Reproduced with permissions [154]. Copyright 2009, Elsevier)

can be also prepared with the addition of inorganic species including MWNTs, Ag, TiO2 and etc. Ra and co-workers first time demonstrated the CNFs preparation by embedding MWNTs in the PAN matrix. Further, electrospun Ag/PAN nanofibers were obtained at the Ag content of 0-5 wt% [158]. Recently, Inagaki et al. reviewed the systematic process for CNF fabrication [151]. Preparation and applications of CNFs prepared by electrospinning have also been reviewed elsewhere [152].

Indeed, carbon nanofibers are currently available on a large scale for a large number of potential applications like field emission sources, catalyst substrate, hydrogen storage, chemical sensors, electrode material, scanning probe tip, nano-electronics and mechanical reinforcements.

10.7 Synthesis of Graphene

Since its discovery in 2004, graphene is being considered as a wonder material for a wide range of potential applications. The unique properties of graphene make it emerging materials for high-speed electronics, optical devices, energy storage, chemical sensors, thermal management and electromagnetic interference shielding applications [11, 12, 159–166]. Optimization of graphene synthesis using various top-down and bottom approach has led to an extraordinary amount of interest in both industry and academics. To date, graphene and graphene oxide has been synthesized from various top-down and bottom-up approaches. In this section, different methods will be discussed for the synthesis of graphene, including the recent developments.

10.7.1 Top-Down Approach

In this approach, graphite is being used as starting materials. Graphite is constructed from sp^2 hybridized carbon atoms arranged in honeycomb lattice structure with an interlayer distance of 3.35 Å along the c-axis. In graphite, all carbon layers bonded together with a weak Van der Waals force. Therefore, graphite can easily exfoliate by either chemical or mechanical exfoliation methods.

10.7.1.1 Mechanical Exfoliation of Graphite

The first single layer of graphene was identified using micromechanical cleavage of highly oriented pyrolytic graphite (HOPG) in 2004 [159]. This method involved an adhesive tape to peel off the graphene layers from HOPG. The peel-off process was repeated many times to achieve a single layer of graphene on tape, followed by transfer on a cleaned substrate [167]. Figure 10.20a showed the optical images of graphene and few-layer graphene deposited on a 300 nm SiO_2 substrate. The thick layer graphene appeared yellow. Upon reduction of the graphene layer thickness, it

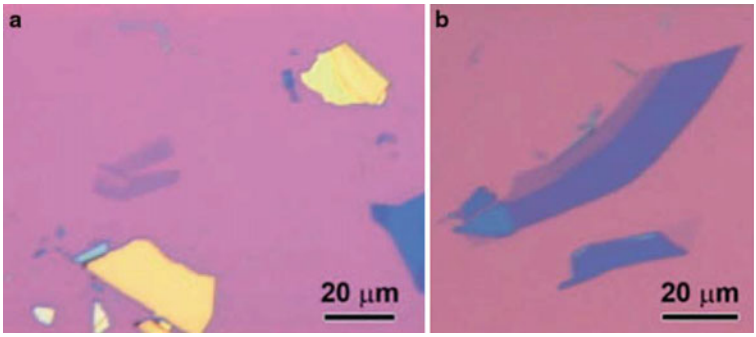

Fig. 10.20 Optical image of exfoliated graphene obtained from the Scotch-tape method. (Reproduced with permissions [168]. Copyright 2010, Elsevier)

showed bluishly. The darker side showed a few layers graphene, while lighter shades showing the single-layer graphene [168]. This micromechanical cleavage process is known as the "Scotch-tape method", which facilitated the initial experimental measurements on the exceptional electronic, thermal conductivity, mechanical and optical properties of graphene. These unique properties generated a huge interest in graphene in almost all branches of science. This Scotch-tape can produce single-layer graphene up to 1 mm with a minimal defect. The produced graphene is good in quality but bulk production is not possible. Therefore, for real-life applications, other synthesis methods are required which can have produced graphene on large scale.

10.7.1.2 Solution-Based Exfoliation of Graphite

Solution exfoliation of graphite has emerged with great interest because it can give producible results on a scalable large scale. Similar to the direct dispersion of carbon nanotubes, many authors directly dispersed the graphite into various organic solvents and then sonicated for exfoliation into a single-layer or multilayer graphene sheets. Coleman et al. obtained good quality graphene sheets by dispersion and sonication of graphite into the NMP solvent [169]. Graphene dispersion was further achieved by 3 h ultrasonication of HOPG in DMF [170]. Various polar and no-polar solvents were explored for graphene synthesis [171]. Bulk production can be achieved by this solution exfoliation method but the production yield is very low. A further attempt was made to ultrasonication-free exfoliation by intercalating graphite with alkaline metals [172]. A high yield of graphene up to 2 mg/mL was obtained by spontaneous exfoliation of HOPG in chlorosulfonic acid [173]. Graphene synthesis in aqueous was also explored by using various surfactants [174, 175]. The analysis confirmed the synthesis of single or few-layer graphene up to a size of a few mm. However, exfoliated graphene sheets are less stable in water in comparison with organic solvents. Graphene synthesis using the solvent exfoliation method depends on many factors

like the size of graphite flakes, sonication time and centrifugation conditions and the solvents. From an industrial point of view, this method is appealing but this solution-based exfoliation approach has several drawbacks. Most of the exfoliated flakes possess a multilayer structure, which gives low yield and large size and thickness heterogeneity among the exfoliated flakes. Moreover, long-time sonication reduces the size of the graphene sheets, resulted in small size graphene sheets, which can significantly affect the properties of graphene sheets. Also, surfactant exfoliated graphene sheets can alter the resulting electronic properties of graphene.

10.7.1.3 Electrochemical Exfoliation of Graphite

After the development of the solution-based exfoliation method, there is a continuous demand for new approaches for the bulk production of high-quality graphene. Then, the researchers developed an electrochemical method for graphene synthesis. The purpose of electrochemical methods is to intercalate the ions within graphite and improve the yield of graphene production [176]. The use of intercalating agents provides an attractive way to exfoliate graphite while retaining the basic properties of graphene. This method involves the application of anodic (oxidation) or cathodic (reduction) potentials in an electrolytes solution, graphitic material as working electrode, reference electrode (SCE, Ag/AgCl, etc.) and a counter (usually Pt) electrodes. The most common and widely studied intercalated ions are Li^+, Ni^{2+}, F^-, $SO_4{}^{2-}$, NO^{3-}, Cl^-, etc. [177]. Several electrolytes and electrochemical conditions were applied to achieve the bulk exfoliation of graphene [178, 179]. It was found that applied potential and electrolytes strongly affected the quality of graphene. Few studies showed that the use of high voltages promotes the formation of oxygen groups on graphene sheets surface and also damages the structure. Graphite intercalation in aqueous SDS surfactant solution explored to drive the exfoliation process. The resulted graphene sheets were found to have a size of 500 and 1 nm thickness was successfully obtained [180]. To avoid the formation of oxygen functionalities on the graphene surface, the cathodic reduction/intercalation method was also attempted [181]. Recently, Adriano and co-workers prepared graphene sheets from commercially available graphite foil as shown in Fig. 10.21a [182]. Three different electrolytes; H_2SO_4, $LiClO_4$ and Na_2SO_4 were tested with a common exfoliation procedure. Optical images of graphite foil before exfoliation and after applying the +10 V potential for prolonged time are shown in Fig. 10.21b, c, respectively. As obtained graphene dispersion in NMP is shown in Fig. 10.21d. Figures 10.21e, f show the exfoliation process at the time of zero, 5 min and 20 min, respectively. As obtained exfoliated graphene was easily dispersible and formed stable dispersion in DMF at the concentration of 1 mg/mL. It was noticed that out of three different electrolytes used in the exfoliation process, either H_2SO_4 or Na_2SO_4 have shown more vigorous and efficient exfoliation.

In comparison with micromechanical cleavage and solvent exfoliation, graphene synthesis using electrochemical exfoliation is more environmentally friendly and generally fast. However, this method also not providing homogenous graphene

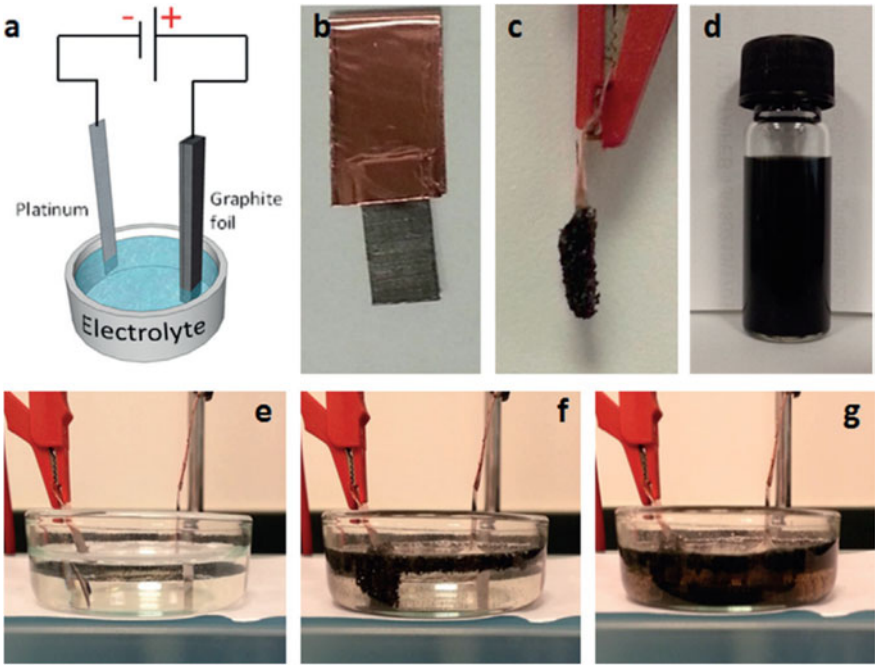

Fig. 10.21 **a** Two electrode electrochemical exfoliation set up, **b** photo of graphite foil before exfoliation, **c** graphite foil after exfoliation process, **d** graphene dispersion in DMF solution (1 mg/ml). **e**, **f** illustrating the exfoliation process at a time (e) zero, (f) after 5 min and (g) after 20 min (Reproduced with permissions [182]. Copyright 2015, Wiley–VCH)

sheets. Also, the use of anodic conditions for ions intercalation causes unwanted oxygen-containing functional groups, which disrupt the sp^2-hybridized carbon structure.

10.7.1.4 Chemical Exfoliation and Reduction

In the chemical exfoliation method, chemical species intercalated within graphitic layers and oxidized the graphitic layers. A little energy in the form of sonication or shaking results as single-layer graphene oxide. Brodie (1859) reported the first successful oxidation of graphite by using potassium chlorate as an oxidizing agent in the presence of nitric acid (HNO_3) [183]. He attempted to establish an exact formula of graphite by producing highly oxidized graphite. He found that the overall mass of graphite flakes was increased upon oxidization due to the presence of hydrogen and oxygen on graphene sheets. This method was further improved by adding chlorate into fuming during the reaction [184]. Further, concentrated sulphuric acid was also added into the mixture to increase oxidization.

Later on, Hummers and Offeman developed another effective oxidation method in which graphite flakes react with the mixture of potassium permanganate ($KMnO_4$) and sodium nitrate in concentrated sulfuric acid (H_2SO_4) with improved experimental safety [19]. This method is considered the primary route for GO preparation and became more popular for the synthesis of graphene. Some researchers have developed slightly modified versions of Hummer's method to avoid the poisonous nitrous gas, which evolves during the reaction in the presence of sodium nitrate in the mixture. After complete oxidation, the interlayer distance between graphitic layers increased to 6 Å or more which is due to the presence of oxygen-containing functional groups on its surface and edges. This increased interlayer distance in graphite oxide weakens the force between layers, can produce a separate layer upon sonication [185]. The separated layers are called graphene oxide (GO). By using this method, a bulk amount of GO can be produced, which is required for commercial applications [186]. Graphene oxide can be dispersed easily in aqueous as well as in organic solvents. But, the main problem with GO is its electrical insulator nature, which is due to the presence of oxygen-containing functional groups on its surface and edges. A lot of research has been performed on GO and its composite materials [187–192]. FESEM images of large size GO prepared by modified Hummer's method is shown in Fig. 10.22a. Figure 10.22b showed its size distribution [188]. More than 50 μm graphene sheets can be synthesized. Size selections of GO sheets strongly depend on the lateral size of graphite flakes and separation conditions. The thickness of as-prepared GO sheets was measured to be ~1 nm (Fig. 10.22c) [189]. The increased thickness of GO sheets is because of oxygen functional groups on the graphene basal plane and edges.

The first serious mechanism of GO synthesis was investigated by Tour and coworkers [193]. In this study, they explained the step-by-step synthesis of graphite into GO as shown in Fig. 10.23. The first step is showing the intercalation of sulphuric acid into graphite, the second step is to covert the intercalated graphite into oxidized graphite and the last step is to exfoliate the graphite oxide into graphene oxide (GO). The study also showed the single-layer GO yield is depending on the oxidation degree of GO sheets. For example, Kim et al. obtained the three different sizes of GO sheets by using different sizes of graphite flakes with variable oxidation time and studied their size-dependent liquid crystalline properties [194]. Production of single-layer GO can be improved by using pre-oxidized graphite flakes. Single-layer GO yield also improved by exfoliation of graphite in presence of tetrabutylammonium ions. However, the process is very time taking [195]. A low-temperature approach was also established for the large production of single-layer GO [196]. Most of the established chemical exfoliation methods used hazardous chemicals, which release poisonous gases. By using the K_2FeO_4 oxidation agent, a 100% yield of GO synthesis was achieved within a short reaction time of 1 h [197]. Similar to other chemical exfoliation methods, this method also releases harmful gases.

The chemically exfoliated graphene oxide has oxygen-containing functional groups on its surfaces. The present functional groups can help for the dispersion of other inorganic nanomaterials and further functionalization of GO for composites and other potential applications. However, graphene oxide sheets are insulating in

nature due to oxygen-containing functional groups. To make it conductive, which is required for most of the graphene applications, we need to remove or reduce these oxygens containing functional groups from the GO surface. There are mainly three common approaches that are being used for such reduction of GO, namely, thermal, chemical and electrochemical reduction methods.

In a thermally reduced approach, GO is annealed at high temperature (1000–2000 °C) under inert conditions. In this method, gaseous species are generated within the interlayers of the GO structures, thin-film/powder and consequently removal of oxygen functional groups and simultaneous graphitization at elevated temperatures, resulting in highly conducting products [198, 199]. Many researchers reported that thermally reduced graphene can improve its electrical and thermal conductivity, but reduced graphene oxide sheets have shown some defects. For example, Xin et al. produced free-standing graphene paper via thermal reduction and graphitization at a very high temperature ~2200 °C [200]. As prepared free-standing graphene paper showed high thermal conductivity of 1238 W/mK. This high temperature thermal annealing approach is straight forward. Thermally reduced graphene oxide has a great potential be used for composite materials, EMI shielding, electrochemical devices

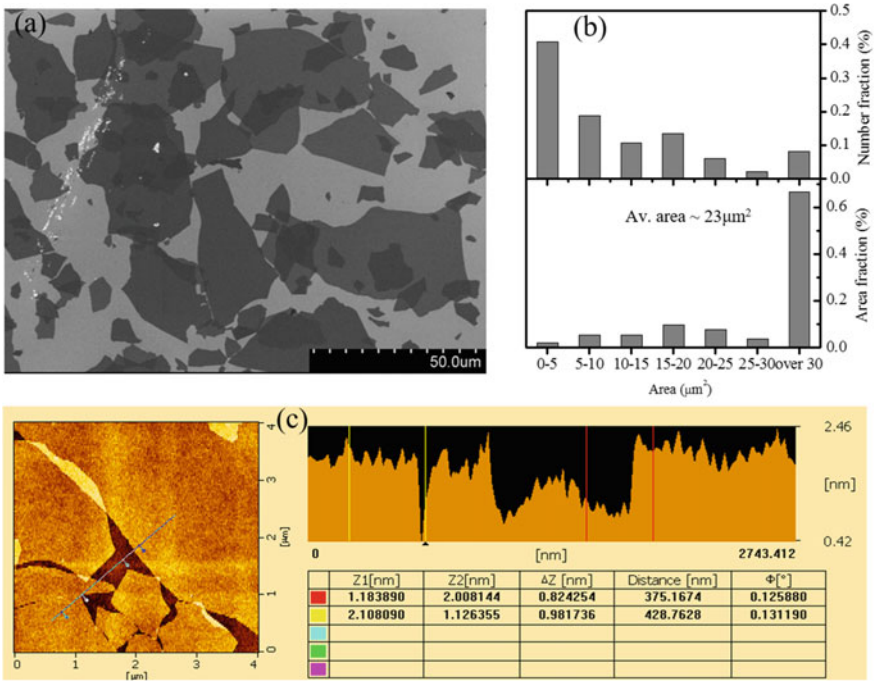

Fig. 10.22 **a** Representative SEM micrograph of large-area GO, **b** size distribution of GO sheets and **c** AFM image of GO sheet (Reproduced with permissions [188, 189]. Copyright 2014, 2015, Elsevier)

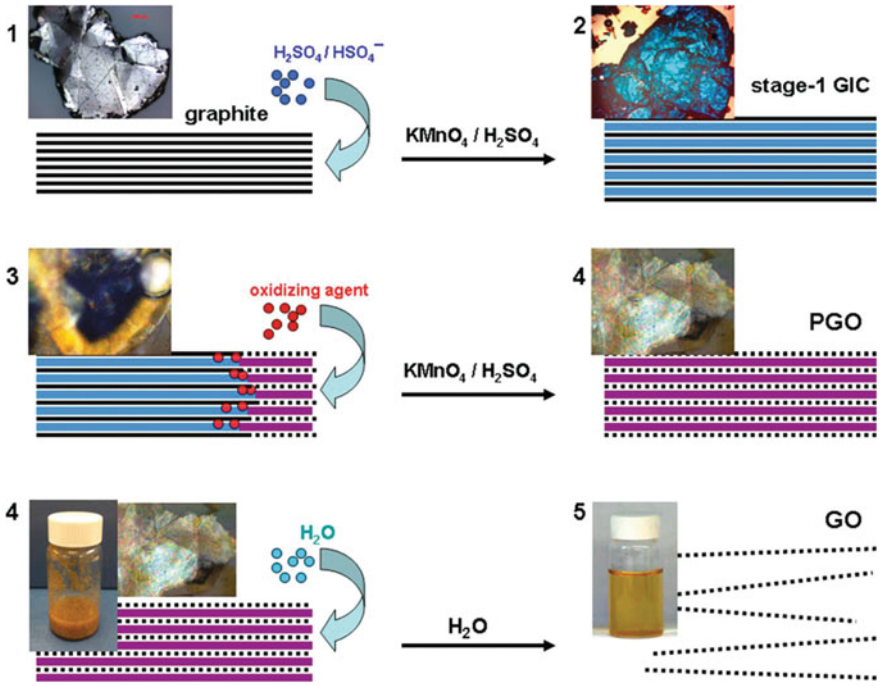

Fig. 10.23 Mechanism of graphite exfoliation into single-layer GO (Reproduced with permissions [193]. Copyright 2014, American Chemical Society)

and conductive ink and paint. But this method has some drawbacks of long-time heating and annealing at high temperature.

Electrochemical reduction of GO is another approach, which can be performed at ambient conditions. Many authors have obtained the pristine graphene-like properties from electrochemically reduced GO [201–203]. Recently, Ambrosi et al. studied the reduction of GO using the electrochemical method, which gives precise control of C/O ratio between 3 to 10 [204]. Thermal and electrochemical reduction methods can reduce GO significantly, however, a chemical reduction is the most widely used method for GO reduction. A chemical reaction/reduction is performed on aqueous GO solution, powder and thin films to remove most of the functional groups. The most studied chemical reducing agent is hydrazine, which was already tested in past in 1937 by Hofmann and König [205]. Beceril et al. investigated GO film reduction by immersing it into a hot aqueous hydrazine solution. In other studies, hydrazine vapor is used for GO reduction even at room temperature. Another reducing agent, $NaBH_4$ was also explored, but all these methods give rigid and fragile rGO films with low electrical conductivity [208]. Experimental findings revealed that both hydrazine and $NaBH_4$ are not effective in reducing agents for GO powder or films. Also, the hydrazine reduction mechanism is not clearly understood.

Further, a more significant route was developed by using halogen hydrohalic acids, which can give highly conductive rGO films [209]. The reduced GO film maintains its flexibility and mechanical strength. Recently, many other reducing agents such as lithium aluminum hydride, hydroxylamine, eco-friendly L-ascorbic acid, saccharides, have been developed for GO reduction [210–213]. Other ways of reducing like a camera flash, UV light and laser scribes were also used for the reduction of GO films [214–216]. It was noticed that chemical reduction procedures can give sufficient electrical, thermal and mechanical properties, however, overall performance is poor compare to pristine graphene. This poor performance of chemically reduced GO is due to incomplete removal of functional groups and the creation of defects on the graphene sheet during the reduction reaction. However, with this poor performance of reduced GO, the chemical reduction method is most widely used for bulk synthesis of reduced GO, which has shown good results in energy storage, sensor and composite applications. For example, Kumar et al. reported the much-improved electrical conductivity of ~3000 S/m and ultrahigh in-plane thermal conductivity of ~19.5 W/mK from low-temperature HI reduced composite film [162].

10.7.1.5 Unzipping Carbon Nanotubes

Unzipping of CNTs can produce graphene. This approach mainly produced different kinds of graphene, called graphene nanoribbons (GNRs) [217, 218]. The typical width of the GNRs is $\leq$50 nm with an aspect ratio of more than 10. Dai et al. reported the GNRs synthesis using partially embedded multiwalled CNTs (MWCNTs) in a PMMA film under an Ar plasma treatment for the various duration [217]. As-prepared GNRs exhibit smooth edges with a narrow width of 10–20 nm (Fig. 10.24). The yield of GNRs is nearly 100% in this method. The resulting graphene nanoribbons contained oxygen functional groups, which can be removed either chemically or thermal annealing method. In contrast to the above work, Tour and co-workers proposed a more scalable approach to open the MWCNTs longitudinally by oxidizing them in presence of sulphuric acid and potassium permanganate [219]. The resulted GNRs exhibited functional groups on their surface. To reduce the defects and vacancies on the GNRs surface, H_3PO_4 was introduced in the oxidation process [218]. Heating of MWNTs in presence of potassium resulted in lower defects on GNRs surface.

Various other methods have been proposed for GNRs synthesis including metal catalyst assisted cutting, thermal exfoliation step, lithium insertion and mechanical sonication in organic solvents [221–225]. Li et al. demonstrated effective intercalation of MWCNTs for the scalable synthesis of GNRs [225]. GNRs have also synthesized the intercalation of Li-NH_3 into MWCNTs and thermal exfoliation [226]. Another interesting approach for GNRs synthesis is catalytic nano-cutting of CNTs [224]. This nano-cutting approach can produce partial or complete unzipping of carbon nanotubes. This technique has some advantages like smooth and sharp edges GNRs with specific orientations can be obtained on large scale. However, the major problem of this technique is that it does not ensure complete cutting in all MWCNTs,

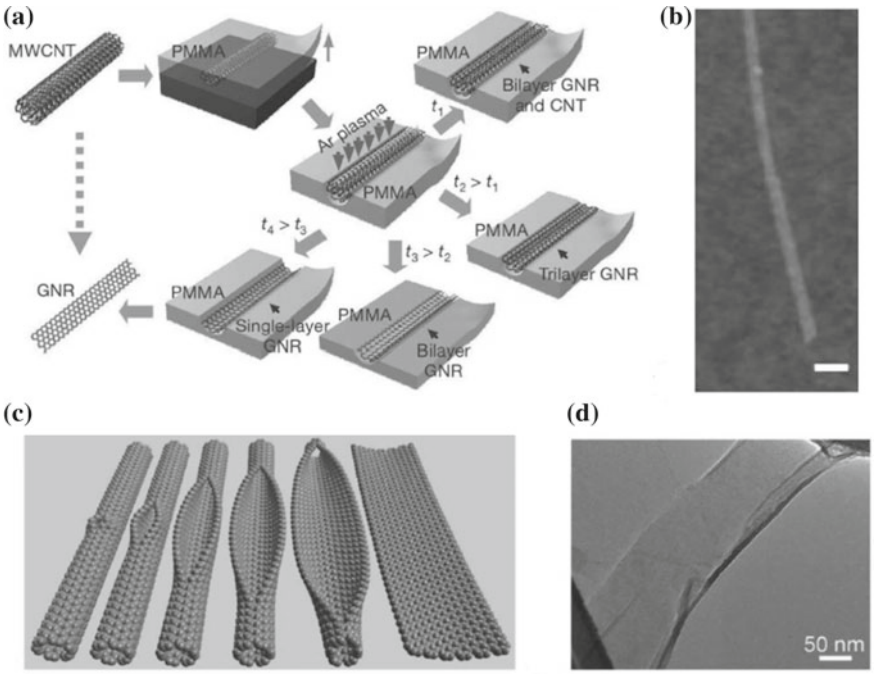

Fig. 10.24 Schematic for GNRs synthesis from unzipping of CNTs with representative TEM images (Reproduced with permissions [221]. Copyright 2010, Wiley–VCH)

which limits its applicability. Synthesis of GNRs without any chemical or catalyst contamination was reported using high DC pulses by using MWCNTs as starting materials [227].

10.7.2 Bottom-Up Methods

This method is mainly based on small molecules to combine by a catalytic process to produce a high-quality graphene sheet [228]. In the first half of the twentieth century, Scholl and Clar pioneered the synthesis of polycyclic aromatic hydrocarbons. Clar et al. (in 1958) firstly synthesized a small graphene sheet with 42 carbon atoms [229]. After that, a series of polycyclic aromatic hydrocarbons with a much larger sp^2 system was proposed [230]. In this route, first branched oligophenylenes were prepared by Diels–Alder reactions and then subjected to oxidative cyclo-dehydrogenation to give planar graphene disks. Under specific conditions, carbon-containing molecules combined into an sp^2-hybridized carbon network. Further, an attempt of graphene synthesis was made using chemical vapor deposition (CVD) and epitaxial growth [231]. These early efforts on the synthesis of monolayer graphene were followed by

a large number of scientists [232]. In this section, synthesis aspects of the bottom-up methods for graphene, specifically, CVD and epitaxial growth approach will discuss.

10.7.2.1 Chemical Vapor Deposition

CVD is a well-established technique for controlled synthesis of various carbon nanomaterials including CNTs, fibers, fullerenes. This method involves the decomposition of carbon sources on transition metal catalyst deposited wafer at high temperature. The decomposed carbon atoms are deposited and then assembled at high temperatures. Large-area epitaxial graphene films (up to a size of few mm) can be obtained. CVD grown graphene was first reported in 2008 and 2009, using Ni and Cu substrates, which was followed by grown over several metal substrates such as iridium, ruthenium, platinum [233–237]. This technique demonstrated the synthesis of single-crystal graphene domains currently up to dimensions of the size in centimeters [238]. The graphene quality was comparable to the Scotch off method produced graphene.

Graphene grown on nickel and copper metal substrates is more popular in comparison with other metal substrates [231, 239, 240]. For graphene growth on a nickel substrate, first polycrystalline Ni films were annealed in Ar/H_2 atmosphere at 900–1000 °C to increase grain size and then the H_2/CH_4 gas mixture was exposed to the substrate. This step involves the decomposition precursor gas and then decomposed carbon atoms dissolve into the Ni film to form a solid solution. Finally, the samples were allowed to cool down in Ar gas. Figure 10.25a illustrates the growth process of graphene on the Ni surface [241]. Ni surface would be an excellent lattice-matched substrate for graphene growth because Ni (111) has a lattice similar to the densely packed hexagonal lattice of graphene (Fig. 10.25b) and they also have similar lattice constants [242]. As-prepared graphene on Ni substrate can be transferred to the required substrate for further study and applications. A low-magnified TEM image of graphene with step-shaped edges is shown in Fig. 10.25c. The inset figure showed the SAED pattern of graphene along the [001] direction. Graphene can main its original structure after transfer on another substrate as shown in Fig. 10.25d. Lewis et al. have also grown graphene on patterned Ni films for desired geometries at specific positions [243]. Wafer-scale graphene synthesis on evaporated Ni films was also demonstrated [239]. It was also demonstrated that the feasibility of transferring graphene on a flexible and transparent substrate has been employed for large-scale flexible transparent electronics applications (Fig. 10.25f) [244]. Tuning of experimental conditions such as deposition temperature, pressure, type and quality of metal substrates and cooling time can improve the graphene growth up to mm scale [245, 246].

Despite good progress in the growth of CVD graphene, there are still many challenges to be overcome for their practical applications. For example, removal of metal catalyst and transfer onto a different arbitrary surface. Thus, the research has been focused on the transfer process of CVD grown graphene on different surfaces. The

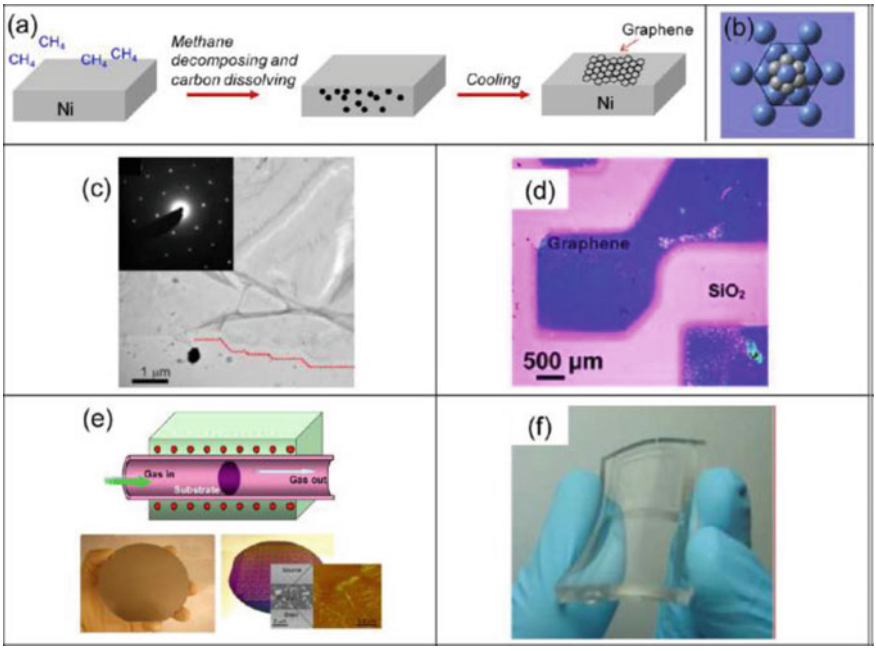

Fig. 10.25 **a** Schematic of graphene formation on Ni substrate, **b** Schematic diagram of graphene atoms (smaller atoms) on Ni (111) lattice (larger atoms), **c** Low magnification TEM image of graphene edges, **d** Optical image of graphene transferred from the Ni surface to SiO_2/Si substrate, **e** Full-wafer-scale deposition of graphene layers on polycrystalline Ni and **f** Flexible and transparent graphene films on the PDMS substrates (Reproduced with permissions [247]. Copyright 2013, American Chemical Society)

transfer of CVD graphene onto arbitrary substrate was obtained using polymer-supported metal etching/transfer or mechanical exfoliation with special functionalized polymers [248]. However, the transfer process usually causes some wrinkles or structural damages, which degrade the quality of graphene [249]. One of the most common transfer methods is the etching of metal substrate while the graphene is supported by an inert polymer such as PMMA or PDMS [247, 250]. So far, several other substrates like PVC, PTFE, PC, CN/CA, PET, paper and cotton cloth have been investigated and applied via a hot/cold lamination process [251]. After complete etching of the metal substrate, the graphene is transferred to the desired substrate followed by the removal of the supporting inert polymer. However, this procedure is very sensitive because it can induce mechanical stress to cause structural damages and alterations. This process also gives some contamination by metallic impurities, which can dramatically alter the electronic properties of the transferred graphene [252, 253]. For example, nickel and copper metal substrates dissolved by etching agents such as $FeCl_3$, $Fe(NO_3)_3$ contaminate the transferred graphene with a significant amount of Fe impurities [254, 255]. Moreover, the incomplete etching process

also can contaminate CVD graphene with an extremely large number of redox-active residuals, such as Cu or Ni metals. Recently, PMMA-graphene was separated from the growth substrates without etching by inducing O_2 bubble generation with a mixture of NH_4OH, H_2O_2 and H_2O [256]. Further, Gao et al. developed a face-to-face transfer of wafer-scale graphene films [257]. This novel approach was based on nascent gas bubbles and capillary bridges that provide high-quality graphene with fewer defects. Several improved techniques were developed such as plasma-enhanced chemical vapor deposition (PECVD) and microwave-assisted CVD for the high-quality fabrication of graphene [258]. Therefore, CVD has been considered as the most versatile and commercially viable technique for the manufacturing of continuous graphene films to meet the industrial demand for electronic-grade materials.

10.7.2.2 Epitaxial Growth

Similar to CVD, the epitaxial technique is also a substrate-based technique in which single-layer graphene is used to grow on a single-crystal carbide (SiC) by vacuum graphitization. The thermal treatment of SiC under vacuum results in the sublimation of the silicon atoms while the carbon-enriched surface rearranges to form graphitic layers (epitaxial graphene). Precise control of the sublimation may lead to the formation of very thin graphitic layers over the entire surface of SiC wafers, with an occasional monolayer of graphene. Recently, a wafer-scale coating of monolayer graphene was achieved by annealing at a higher temperature (1650 °C) under the Ar atmosphere rather than 1150 °C under UHV conditions [259]. The obtained wafer-scale monolayered graphene exhibited carrier mobility of 2000 cm^2/Vs at room temperature for a carrier density of ~10^{13} cm^2. This value is only five times lesser than the mechanically exfoliated graphene. Some other researchers have also reported the mechanisms and kinetics of epitaxial graphene growth on SiC [260, 261]. A schematic of the synthesis process is shown in Fig. 10.26 [262]. Epitaxial growth on SiC can be achieved by an additional supply of carbon without subliming

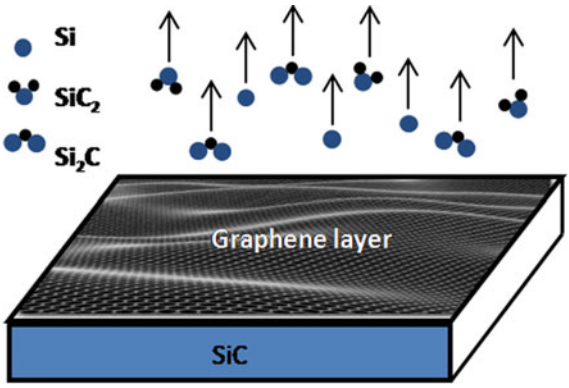

Fig. 10.26 Epitaxial graphene growth on silicon carbide wafer via sublimation of silicon atoms (Reproduced with permissions [262]. Copyright 2016, Wiley–VCH)

Si. This additional supply of carbon may be given by hydrocarbon gas decomposition or by sublimation of solid carbon source in molecular beam epitaxy [263]. Apart from SiC, other carbides have been exploited early on to fabricate supported graphene. Successful preparation of graphene monolayers has been achieved on the (100), (111) and (410) surfaces of titanium and the (111) faces of tantalum by decomposition of ethylene gas [264]. Interestingly the morphology of the TiC faces determines the graphene structure. In particular, monolayer graphene nanoribbons were obtained on the 0.886 nm-wide terraces of TiC(410), while large monolayer crystallites were formed on terrace-free TiC (111). It should be noted that SiC is a wide bandgap semiconductor and no transfer of graphene is required on other substrates, which allows very easy fabrication of the devices. Therefore, epitaxially grown graphene is very promising for the mainstream electronics industry. However, this technique has some limitations for large-scale fabrication due to the high cost of single-crystal SiC wafers. Another challenge in this technique is the uniform growth of large-area single-layer graphene.

Graphene has been considered as one of the most promising materials for a wide range of applications not only because of its excellent electronic, optical, thermal and mechanical properties but also due to its easy synthesis and handling for technology transfer. The unique properties of graphene make it useful in most areas including environment, sensors, solar cells, supercapacitor, batteries, fuel cell and catalysis [265–267]. Chemical exfoliation and reduction procedure can produce a single layer on a large scale which is mainly required for most industrial applications. Nevertheless, CVD produced graphene has shown promising results for electronic/device applications.

Conclusion

This chapter gives clear indications on the synthesis of various carbon materials Several synthesis methods like soot, arc discharge, chemical vapor deposition, mechanical and chemical exfoliation, electrospinning and epitaxial growth have been highlighted. The growth mechanism for all carbon materials has been discussed. Among carbon-based materials, graphene is a newly invented material with ultimate properties. Therefore, high-quality graphene synthesis by various routes in important for different kinds of applications.

References

1. Andresen JM (2001) Graphite and precursors, world of carbon. In: Delhaès P (ed) vol 1. Gordon and Breach Publishers, Amsterdam, p 297. ISBN 90-5699-228-7. $85, Energy & Fuels 16(1):218-218
2. Vavilov VS (1997) Diamond in solid state electronics. Phys Usp 40:15–20
3. Wild C, Müller-Sebert W, Eckermann T, Koidl P (1991) Polycrystalline diamond films for optical applications. In: Tzeng Y, Yoshikawa M, Murakawa M, Feldman A (eds) Materials science monographs. Elsevier, pp 197–205
4. Kroto HW, Heath JR, O'Brien SC, Curl RF, Smalley RE (1985) C60: Buckminsterfullerene. Nature 318(6042):162–163

5. Iijima S (1991) Helical microtubules of graphitic carbon. Nature 354(6348):56–58
6. Prasek J, Drbohlavova J, Chomoucka J, Hubalek J, Jasek O, Adam V, Kizek R (2011) Methods for carbon nanotubes synthesis—review. J Mater Chem 21(40):15872–15884
7. De Volder MFL, Tawfick SH, Baughman RH, Hart AJ (2013) Carbon nanotubes: present and future commercial applications. Science 339(6119):535–539
8. Yadav D, Amini F, Ehrmann A (2020) Recent advances in carbon nanofibers and their applications – a review. Euro Polymer J 138:109963
9. Novoselov KS, Geim AK, Morozov SV, Jiang D, Zhang Y, Dubonos SV, Grigorieva IV, Firsov AA (2004) Electric field effect in atomically thin carbon films. Science 306(5696):666–669
10. Allen MJ, Tung VC, Kaner RB (2010) Honeycomb carbon: a review of graphene. Chem Rev 110(1):132–145
11. Kumar P (2019) Ultrathin 2D nanomaterials for electromagnetic interference shielding. Adv Mater Interfaces 6(24):1901454
12. Yadav MK, Panwar N, Singh S, Kumar P (2020) Preheated self-aligned graphene oxide for enhanced room temperature hydrogen storage. Int J Hydrogen Energy 45(38):19561–19566
13. Vikas, Yadav MK, Kumar P, Verma RK (2020) Detection of adulteration in pure honey utilizing Ag-graphene oxide coated fiber optic SPR probes. Food Chem 332:127346
14. Avouris P, Dimitrakopoulos C (2012) Graphene: synthesis and applications. Mater Today 15(3):86–97
15. Edwards RS, Coleman KS (2013) Graphene synthesis: relationship to applications. Nanoscale 5(1):38–51
16. Baddour CE, Fadlallah F, Nasuhoglu D, Mitra R, Vandsburger L, Meunier J-L (2009) A simple thermal CVD method for carbon nanotube synthesis on stainless steel 304 without the addition of an external catalyst. Carbon 47(1):313–318
17. Ritter S (2001) PENCILS & PENCIL LEAD. Chem Eng News Arch 79(42):35
18. Arregui-Mena JD, Bodel W, Worth RN, Margetts L, Mummery PM (2016) Spatial variability in the mechanical properties of Gilsocarbon. Carbon 110:497–517
19. Hummers WS, Offeman RE (1958) Preparation of graphitic oxide. J Am Chem Soc 80(6):1339–1339
20. Kawamoto M, He P, Ito Y (2017) Green processing of carbon nanomaterials. Adv Mater 29(25):1602423
21. Strong HM (1989) Strong, early diamond making at general electric. Am J Phys 57:794
22. Gogotsi YG, Kofstad P, Yoshimura M, Nickel KG (1996) Formation of sp3-bonded carbon upon hydrothermal treatment of SiC. Diam Relat Mater 5(2):151–162
23. Shenderova OA, Shames AI, Nunn NA, Torelli MD, Vlasov I, Zaitsev A (2019) Review article: synthesis, properties, and applications of fluorescent diamond particles. J Vacuum Sci Technol B 37(3):030802
24. Schwander M, Partes K (2011) A review of diamond synthesis by CVD processes. Diam Relat Mater 20(9):1287–1301
25. Kobashi K, Nishimura K, Kawate Y, Horiuchi T (1988) Synthesis of diamonds by use of microwave plasma chemical-vapor deposition: morphology and growth of diamond films. Phys Rev B 38(6):4067–4084
26. Liu X, Jia X, Zhang Z, Li Y, Hu M, Zhou Z, Ma H-A (2011) Crystal growth and characterization of diamond from carbonyl iron catalyst under high pressure and high temperature conditions. Cryst Growth Des 11(9):3844–3849
27. Palyanov YN, Kupriyanov IN, Borzdov YM, Sokol AG, Khokhryakov AF (2009) Diamond crystallization from a sulfur−carbon system at HPHT conditions. Cryst Growth Des 9(6):2922–2926
28. Palyanov YN, Kupriyanov IN, Borzdov YM, Khokhryakov AF, Surovtsev NV (2016) High-pressure synthesis and characterization of Ge-doped single crystal diamond. Cryst Growth Des 16(6):3510–3518
29. Palyanov YN, Kupriyanov IN, Sokol AG, Khokhryakov AF, Borzdov YM (2011) Diamond growth from a phosphorus–carbon system at high pressure high temperature conditions. Cryst Growth Des 11(6):2599–2605

30. Hu M, Ma H-A, Yan B, Li Y, Li Z, Zhou Z, Jia X (2012) Multiseed method for high quality sheet cubic diamonds synthesis: an effective solution for scientific research and commercial production. Cryst Growth Des 12(1):518–521
31. Ashfold MNR, May PW, Rego CA, Everitt NM (1994) Thin film diamond by chemical vapour deposition methods. Chem Soc Rev 23(1):21–30
32. Holland L, Ojha SM (1979) The growth of carbon films with random atomic structure from ion impact damage in a hydrocarbon plasma. Thin Solid Films 58(1):107–116
33. Angus JC, Will HA, Stanko WS (1968) Growth of diamond seed crystals by vapor deposition. J Appl Phys 39(6):2915–2922
34. Rakha SA, Xintai Z, Zhu D, Guojun Y (2010) Effects of N2 addition on nanocrystalline diamond films by HFCVD in Ar/CH4 gas mixture. Curr Appl Phys 10(1):171–175
35. Kondoh E, Ohta T, Mitomo T, Ohtsuka K (1991) Determination of activation energies for diamond growth by an advanced hot filament chemical vapor deposition method. Appl Phys Lett 59(4):488–490
36. Park SS, Lee JY (1991) Synthesis of diamond films on titanium substrates by hot-filament chemical vapor deposition. J Appl Phys 69(4):2618–2622
37. Kobayashi T, Hirakuri KK, Mutsukura N, Machi Y (1999) Synthesis of CVD diamond at atmospheric pressure using the hot-filament CVD method. Diam Relat Mater 8(6):1057–1060
38. Ali M, Ürgen M (2012) Simultaneous growth of diamond and nanostructured graphite thin films by hot-filament chemical vapor deposition. Solid State Sci 14(1):150–154
39. Hirose Y, Amanuma S, Komaki K (1990) The synthesis of high-quality diamond in combustion flames. J Appl Phys 68(12):6401–6405
40. Kamo M, Sato Y, Matsumoto S, Setaka N (1983) Diamond synthesis from gas phase in microwave plasma. J Cryst Growth 62(3):642–644
41. Matsumoto S (1985) Chemical vapour deposition of diamond in RF glow discharge. J Mater Sci Lett 4(5):600–602
42. Kawarada H, Mar KS, Hiraki A (1987) Large area chemical vapour deposition of diamond particles and films using magneto-microwave plasma. Jpn J Appl Phys 26(Part 2, No. 6):L1032–L1034
43. Salvadori MC, Ager JW III, Brown IG, Krishnan KM (1991) Diamond synthesis by microwave plasma chemical vapor deposition using graphite as the carbon source. Appl Phys Lett 59(19):2386–2388
44. Katsumata S (1992) Diamond synthesis by the microwave plasma chemical vapor deposition method using the pretreated carbon dioxide and hydrogen mixed-gas system. Jpn J Appl Phys 31(Part 1, No. 3):868–871
45. Tiwari RN, Tiwari JN, Chang L, Yoshimura M (2011) Enhanced nucleation and growth of diamond film on Si by CVD using a chemical precursor. J Phys Chem C 115(32):16063–16073
46. Liang Q, Yan C-S, Lai J, Meng Y-F, Krasnicki S, Shu H, Mao H-K, Hemley RJ (2014) Large area single-crystal diamond synthesis by 915 MHz microwave plasma-assisted chemical vapor deposition. Cryst Growth Des 14(7):3234–3238
47. Palnichenko AV, Jonas AM, Charlier JC, Aronin AS, Issi JP (1999) Diamond formation by thermal activation of graphite. Nature 402(6758):162–165
48. Szymanski A, Abgarowicz E, Bakon A, Niedbalska A, Salacinski R, Sentek J (1995) Diamond formed at low pressures and temperatures through liquid-phase hydrothermal synthesis. Diam Relat Mater 4(3):234–235
49. Gogotsi YG, Yoshimura M (1994) Formation of carbon films on carbides under hydrothermal conditions. Nature 367(6464):628–630
50. Lou Z, Chen Q, Zhang Y, Wang W, Qian Y (2003) Diamond formation by reduction of carbon dioxide at low temperatures. J Am Chem Soc 125(31):9302–9303
51. Narayan RJ, Boehm RD, Sumant AV (2011) Medical applications of diamond particles & surfaces. Mater Today 14(4):154–163
52. Krätschmer W, Lamb LD, Fostiropoulos K, Huffman DR (1990) Solid C60: a new form of carbon. Nature 347(6291):354–358

53. Huczko A, Lange H, Byszewski P, Poplawska M, Starski A (1997) Fullerene formation in carbon arc: electrode gap dependence and plasma spectroscopy. J Phys Chem A 101(7):1267–1269
54. Howard JB, McKinnon JT, Makarovsky Y, Lafleur AL, Johnson ME (1991) Fullerenes C60 and C70 in flames. Nature 352(6331):139–141
55. McKinnon JT, Bell WL, Barkley RM (1992) Combustion synthesis of fullerenes. Combust Flame 88(1):102–112
56. Reilly PTA, Gieray RA, Whitten WB, Ramsey JM (2000) Fullerene evolution in flame-generated soot. J Am Chem Soc 122(47):11596–11601
57. Chow L, Wang H, Kleckley S, Daly TK, Buseck PR (1995) Fullerene formation during production of chemical vapor deposited diamond. Appl Phys Lett 66(4):430–432
58. Kleckley S, Wang H, Oladeji I, Chow L, Daly TK, Buseck PR, Solouki T, Marshall A (1997) Fullerenes and polymers produced by the chemical vapor deposition method, synthesis and characterization of advanced materials. American Chemical Society, pp 51–60
59. Inomata K, Aoki N, Koinuma H (1994) Production of fullerenes by low temperature plasma chemical vaper deposition under atmospheric pressure. Jpn J Appl Phys 33(Part 2, No. 2A):L197–L199
60. Wang X, Xu B, Liu X, Guo J, Ichinose H (2006) Synthesis of Fe-included onion-like fullerenes by chemical vapor deposition. Diam Relat Mater 15(1):147–150
61. Churilov GN (2008) Synthesis of fullerenes and other nanomaterials in arc discharge, Fullerenes. Nanotubes Carbon Nanostruct 16(5–6):395–403
62. Lieber CM, Chen CC (1994) Preparation of fullerenes and fullerene-based materials. Solid State Phys Adv Res Appl 109–148
63. Caraman M, Lazar JB, Stamate M, La (2008) ARC DISCHARGE INSTALATION FOR FULLERENE PRODUCTION
64. Sundar CS, Bharathi A, Hariharan Y, Janaki J, Sankara Sastry V, Radhakrishnan TS (1992) Thermal decomposition of C60. Solid State Commun 84(8):823–826
65. Wang CZ, Xu CH, Chan CT, Ho KM (1992) Disintegration and formation of fullerene (C60). J Phys Chem 96(9):3563–3565
66. Taylor R, Parsons JP, Avent AG, Rannard SP, Dennis TJ, Hare JP, Kroto HW, Walton DRM (1991) Degradation of C60 by light. Nature 351(6324):277–277
67. Carbon arc solar simulator. Appl Opt 30(10):1290–1293
68. Meubus P (1986) Effects of UV light irradiation on propane in an argon plasma. Plasma Chem Plasma Process 6(2):143–157
69. Parker DH, Chatterjee K, Wurz P, Lykke KR, Pellin MJ, Stock LM, Hemminger JC (1992) Fullerenes and giant fullerenes: synthesis, separation, and mass spectrometric characterization. Carbon 30(8):1167–1182
70. Scrivens WA, Tour JM (1992) Synthesis of gram quantities of C60 by plasma discharge in a modified round-bottomed flask. Key parameters for yield optimization and purification. J Org Chem 57(25):6932–6936
71. Lamb LD, Huffman DR (1993) Fullerene production. J Phys Chem Solids 54(12):1635–1643
72. Yu T, Li J-C, Cai F-X, Fan X-J (1994) Chen M-SYR, Wu W, Xiao N, Tian D-C, Zhao W-K, Fang Y-L, Kuang A-Y. Fullerene Sci Technol 2(3):223–231
73. Koprinarov N, Marinov M, Konstantinova M, Ranguelov B (2000) Fullerene structure synthesis by DC arc discharge in ferrocene vapours. Vacuum 58(2):208–214
74. Chibante LPF, Thess A, Alford JM, Diener MD, Smalley RE (1993) Solar generation of the fullerenes. J Phys Chem 97(34):8696–8700
75. Brusatin G, Signorini R (2002) Linear and nonlinear optical properties of fullerenes in solid state materials. J Mater Chem 12(7):1964–1977
76. He YJ, Chen H-Y, Hou JH, Li YF (2010) Indene−C60 bisadduct: a new acceptor for high-performance polymer solar cells. J Am Chem Soc 132(4):1377–1382
77. Peng P, Li F-F, Neti VSPK, Metta-Magana AJ, Echegoyen L (2014) Design, synthesis, and X-ray crystal structure of a fullerene-linked metal–organic framework. Angew Chem Int Ed 53(1):160–163

78. Figueira-Duarte TM, Clifford J, Amendola V, Gegout A, Olivier J, Cardinal F, Meneghetti M, Armaroli N, Nierengarten J-F (2006) Synthesis and excited state properties of a fullerene derivative bearing a star-shaped multi-photon absorption chromophore. Chem Commun 19:2054–2056
79. Garg V, Kodis G, Chachisvilis M, Hambourger M, Moore AL, Moore TA, Gust D (2011) Conformationally constrained macrocyclic diporphyrin−fullerene artificial photosynthetic reaction center. J Am Chem Soc 133(9):2944–2954
80. Sawamura M, Kawai K, Matsuo Y, Kanie K, Kato T, Nakamura E (2002) Stacking of conical molecules with a fullerene apex into polar columns in crystals and liquid crystals. Nature 419(6908):702–705
81. Inglis AJ, Pierrat P, Muller T, Bräse S, Barner-Kowollik C (2010) Well-defined star shaped polymer-fullerene hybrids via click chemistry. Soft Matter 6(1):82–84
82. Nava MG, Setayesh S, Rameau A, Masson P, Nierengarten J-F (2002) Fullerene-functionalized polyesters: synthesis, characterization and incorporation in photovoltaic cells. New J Chem 26(11):1584–1589
83. Radushkevich LV, Lukyanovich VM (1952) The structure of carbon forming in thermal decomposition of carbon monoxide on an iron catalyst. Russ J Phys Chem 26:88–95
84. Oberlin A, Endo M, Koyama T (1976) Filamentous growth of carbon through benzene decomposition. J Cryst Growth 32(3):335–349
85. Iijima S, Ichihashi T (1993) Single-shell carbon nanotubes of 1-nm diameter. Nature 363(6430):603–605
86. Dresselhaus MS, Dresselhaus G, Saito R (1995) Physics of carbon nanotubes. Carbon 33(7):883–891
87. Arora N, Sharma NN (2014) Arc discharge synthesis of carbon nanotubes: comprehensive review. Diam Relat Mater 50:135–150
88. Seraphin S, Zhou D, Jiao J, Minke MA, Wang S, Yadav T, Withers JC (1994) Catalytic role of nickel, palladium, and platinum in the formation of carbon nanoclusters. Chem Phys Let 217(3):191–195
89. Saito Y, Nishikubo K, Kawabata K, Matsumoto T (1996) Carbon nanocapsules and single-layered nanotubes produced with platinum-group metals (Ru, Rh, Pd, Os, Ir, Pt) by arc discharge. J Appl Phys 80(5):3062–3067
90. Wang H, Li Z, Inoue S, Ando Y (2010) Influence of mo on the growth of single-walled carbon nanotubes in arc discharge. J Nanosci Nanotechnol 10(6):3988–3993
91. Xing G, Jia S, Xing J, Shi Z (2007) Analysis of the carbon nano-structures formation in liquid arcing. Plasma Sci Technol 9:770
92. Shi Z, Lian Y, Liao F, Zhou X, Gu Z, Zhang Y, Iijima S (1999) Purification of single-wall carbon nanotubes. Solid State Commun 112(1):35–37
93. Maschmann MR, Franklin AD, Amama PB, Zakharov DN, Stach EA, Sands TD, Fisher TS (2006) Vertical single- and double-walled carbon nanotubes grown from modified porous anodic alumina templates. Nanotechnology 17(15):3925–3929
94. Hutchison JL, Kiselev NA, Krinichnaya EP, Krestinin AV, Loutfy RO, Morawsky AP, Muradyan VE, Obraztsova ED, Sloan J, Terekhov SV, Zakharov DN (2001) Double-walled carbon nanotubes fabricated by a hydrogen arc discharge method. Carbon 39(5):761–770
95. Sugai T, Yoshida H, Shimada T, Okazaki T, Shinohara H, Bandow S (2003) New synthesis of high-quality double-walled carbon nanotubes by high-temperature pulsed arc discharge. Nano Letter 3(6):769–773
96. Huang HJ, Kajiura H, Tsutsui S, Murakami Y, Ata M (2003) High-quality double-walled carbon nanotube super bundles grown in a hydrogen-free atmosphere. J Phys Chem B 107(34):8794–8798
97. Liu Q, Ren W, Li F, Cong H, Cheng H-M (2007) Synthesis and high thermal stability of double-walled carbon nanotubes using nickel formate dihydrate as catalyst precursor. J Phys Chem C 111(13):5006–5013
98. Li L, Li F, Liu C, Cheng H-M (2005) Synthesis and characterization of double-walled carbon nanotubes from multi-walled carbon nanotubes by hydrogen-arc discharge. Carbon 43(3):623–629

99. Wang M, Zhao XL, Ohkohchi M, Ando Y (1996) Carbon nanotubes grown on the surface of cathode deposit by arc discharge. Fullerene Sci Technol 4(5):1027–1039
100. Parkansky N, Boxman RL, Alterkop B, Zontag I, Lereah Y, Barkay Z (2004) Single-pulse arc production of carbon nanotubes in ambient air. J Phys D Appl Phys 37(19):2715–2719
101. Tsai YY, Su JS, Su CY, He WH (2009) Production of carbon nanotubes by single-pulse discharge in air. J Mater Process Technol 209(9):4413–4416
102. Sornsuwit N, Maaithong W (2008) Study of multi-walled carbon nanotube synthesis using liquid nitrogen and post-process filtration. Int J Precis Eng Manuf 9(3):18–21
103. Montoro LA, Lofrano RCZ, Rosolen JM (2005) Synthesis of single-walled and multi-walled carbon nanotubes by arc-water method. Carbon 43(1):200–303
104. Jung SH, Kim MR, Jeong SH, Kim SU, Lee OJ, Lee KH, Suh JH, Park CK (2003) High-yield synthesis of multi-walled carbon nanotubes by arc discharge in liquid nitrogen. Appl Phys A Mater Sci Process 76(2):285–286
105. Guo J, Wang X, Yao Y, Yang X, Liu X, Xu B (2007) Structure of nanocarbons prepared by arc discharge in water. Mater Chem Phys 105(2):175–178
106. Guo T, Nikolaev P, Thess A, Colbert DT, Smalley RE (1995) Catalytic growth of single-walled manotubes by laser vaporization. Chem Phys Lett 243(1):49–54
107. Yudasaka M, Yamada R, Sensui N, Wilkins T, Ichihashi T, Iijima S (1999) Mechanism of the effect of NiCo, Ni and Co catalysts on the yield of single-wall carbon nanotubes formed by pulsed Nd:YAG laser ablation. J Phys Chem 103(30):6224–6229
108. Thess A, Lee R, Nikolaev P, Dai H, Petit P, Robert J, Xu C, Lee YH, Kim SG, Linzler AG, Colbert DT, Scuseria GE, Tomanek D, Fischer JE, Smalley RE (1996) Crystalline ropes of metallic carbon nanotubes. Science 273(5274):483
109. Bandow S, Asaka S, Saito Y, Rao AM, Grigorian L, Richter E, Eklund PC (1998) Effect of the growth temperature on the diameter distribution and chirality of single-wall carbon nanotubes. Phys Rev Lett 80(17):3779–3782
110. Maser WK, Muñoz E, Benito AM, Martínez MT, de la Fuente GF, Maniette Y, Anglaret E, Sauvajol JL (1998) Production of high-density single-walled nanotube material by a simple laser-ablation method. Chem Phys Lett 292(4):587–593
111. Braidy N, El Khakani MA, Botton GA (2002) Single-wall carbon nanotubes synthesis by means of UV laser vaporization. Chem Phys Lett 354(1):88–92
112. Chen M, Chen C-M, Koo H-S, Chen C-F (2003) Catalyzed growth model of carbon nanotubes by microwave plasma chemical vapor deposition using CH4 and CO2 gas mixtures. Diam Relat Mater 12(10):1829–1835
113. Purohit R, Purohit K, Rana S, Rana RS, Patel V (2014) Carbon nanotubes and their growth methods. Proc Mater Sci 6:716–728
114. Bonaccorso F, Bongiorno C, Fazio B, Gucciardi PG, Maragò OM, Morone A, Spinella C (2007) Pulsed laser deposition of multiwalled carbon nanotubes thin films. Appl Surf Sci 254(4):1260–1263
115. Muñoz E, Maser WK, Benito AM, de la Fuente GF, Martínez MT (1999) Single-walled carbon nanotubes produced by laser ablation under different inert atmospheres. Synth Met 103(1):2490–2491
116. Muñoz E, Maser WK, Benito AM, Martínez MT, de la Fuente GF, Maniette Y, Righi A, Anglaret E, Sauvajol JL (2000) Gas and pressure effects on the production of single-walled carbon nanotubes by laser ablation. Carbon 38(10):1445–1451
117. Hiura H, Ebbesen TW, Tanigaki K (1995) Opening and purification of carbon nanotubes in high yields, Adv Mater 7(3):275–276
118. Varshney D, Weiner BR, Morell G (2010) Growth and field emission study of a monolithic carbon nanotube/diamond composite. Carbon 48(12):3353–3358
119. Tempel H, Joshi R, Schneider JJ (2010) Ink jet printing of ferritin as method for selective catalyst patterning and growth of multiwalled carbon nanotubes. Mater Chem Phys 121(1):178–183
120. Patole SP, Alegaonkar PS, Lee H-C, Yoo J-B (2008) Optimization of water assisted chemical vapor deposition parameters for super growth of carbon nanotubes. Carbon 46(14):1987–1993

121. Brown B, Parker CB, Stoner BR, Glass JT (2011) Growth of vertically aligned bamboo-like carbon nanotubes from ammonia/methane precursors using a platinum catalyst. Carbon 49(1):266–274
122. Andrews R, Jacques D, Qian D, Rantell T (2002) Multiwall carbon nanotubes: synthesis and application. Acc Chem Res 35(12):1008–1017
123. Dumpala S, Jasinski JB, Sumanasekera GU, Sunkara MK (2011) Large area synthesis of conical carbon nanotube arrays on graphite and tungsten foil substrates. Carbon 49(8):2725–2734
124. Ramesh P, Okazaki T, Taniguchi R, Kimura J, Sugai T, Sato K, Ozeki Y, Shinohara H (2005) Selective chemical vapor deposition synthesis of double-wall carbon nanotubes on mesoporous silica. J Phys Chem B 109(3):1141–1147
125. Zhu J, Yudasaka M, Iijima S (2003) A catalytic chemical vapor deposition synthesis of double-walled carbon nanotubes over metal catalysts supported on a mesoporous material. Chem Phys Lett 380(5):496–502
126. Szabó A, Perri C, Csató A, Giordano G, Vuono D, Nagy JB (2010) Synthesis methods of carbon nanotubes and related materials. Materials 3(5):3092–3140
127. Xiang X, Zhang L, Hima HI, Li F, Evans DG (2009) Co-based catalysts from Co/Fe/Al layered double hydroxides for preparation of carbon nanotubes. Appl Clay Sci 42(3):405–409
128. Flahaut E, Laurent C, Peigney A (2005) Catalytic CVD synthesis of double and triple-walled carbon nanotubes by the control of the catalyst preparation. Carbon 43(2):375–383
129. Jiang Q, Song LJ, Yang H, He ZW, Zhao Y (2008) Preparation and characterization on the carbon nanotube chemically modified electrode grown in situ. Electrochem Commun 10(3):424–427
130. Lyu SC, Liu BC, Lee CJ, Kang HK, Yang C-W, Park CY (2003) High-quality double-walled carbon nanotubes produced by catalytic decomposition of benzene. Chem Mater 15(20):3951–3954
131. Tang N, Kuo W, Jeng C, Wang L, Lin K, Du Y (2010) Coil-in-coil carbon nanocoils: 11 gram-scale synthesis, single nanocoil electrical properties, and electrical contact improvement. ACS Nano 4(2):781–788
132. Liu Z, Jiao L, Yao Y, Xian X, Zhang J (2010) Aligned, ultralong single-walled carbon nanotubes: from synthesis, sorting, to electronic devices. Adv Mater 22(21):2285–2310
133. Zhang D, Yan T, Pan C, Shi L, Zhang J (2009) Carbon nanotube-assisted synthesis and high catalytic activity of CeO2 hollow nanobeads. Mater Chem Phys 113(2):527–530
134. Sano N, Ishimaru S, Tamaon H (2010) Synthesis of carbon nanotubes in graphite microchannels in gas-flow and submerged-in-liquid reactors. Mater Chem Phys 122(2):474–479
135. Lim S, Luo Z, Shen Z, Lin J (2010) Plasma-assisted synthesis of carbon nanotubes. Nanoscale Res Lett 5(9):1377
136. Kim SM, Gangloff L (2009) Growth of carbon nanotubes (CNTs) on metallic underlayers by diffusion plasma-enhanced chemical vapour deposition (DPECVD). Phys E 41(10):1763–1766
137. Vollebregt S, Derakhshandeh J, Ishihara R, Wu MY, Beenakker CIM (2010) Growth of high-density self-aligned carbon nanotubes and nanofibers using palladium catalyst. J Electron Mater 39(4):371–375
138. Häffner M, Schneider K, Schuster BE, Stamm B, Latteyer F, Fleischer M, Burkhardt C, Chassé T, Stett A, Kern DP (2010) Plasma enhanced chemical vapor deposition grown carbon nanotubes from ferritin catalyst for neural stimulation microelectrodes. Microelectron Eng 87(5):734–737
139. Rodriguez NM, Chambers A, Baker RTK (1995) Catalytic engineering of carbon nanostructures. Langmuir 11(10):3862–3866
140. Zhou Z, Lai C, Zhang L, Qian Y, Hou H, Reneker DH, Fong H (2009) Development of carbon nanofibers from aligned electrospun polyacrylonitrile nanofiber bundles and characterization of their microstructural, electrical, and mechanical properties. Polymer 50(13):2999–3006
141. Motojima S, Kawaguchi M, Nozaki K, Iwanaga H (1990) Growth of regularly coiled carbon filaments by Ni catalyzed pyrolysis of acetylene, and their morphology and extension characteristics. Appl Phys Lett 56(4):321–323

142. Motojima S, Chen Q (1999) Three-dimensional growth mechanism of cosmo-mimetic carbon microcoils obtained by chemical vapor deposition. J Appl Phys 85(7):3919–3921
143. Zhang M, Nakayama Y, Pan L (2000) Synthesis of carbon tubule nanocoils in high yield using iron-coated indium tin oxide as catalyst. Jpn J Appl Phys 39(Part 2, No. 12A):L1242–L1244
144. Raghubanshi H, Dikio ED (2015) Synthesis of helical carbon fibers and related materials: a review on the past and recent developments. Nanomaterials (Basel, Switzerland) 5(2):937–968
145. Song H, Shen W (2014) Carbon nanofibers: synthesis and applications. J Nanosci Nanotechnol 14(2):1799–1810
146. Minea TM, Point S, Granier A, Touzeau M (2004) Room temperature synthesis of carbon nanofibers containing nitrogen by plasma-enhanced chemical vapor deposition. Appl Phys Lett 85(7):1244–1246
147. Zou J-z, Zeng X-r, Xiong X-b, Tang H-l, Li L, Liu Q, Li Z-q (2007) Preparation of vapor grown carbon fibers by microwave pyrolysis chemical vapor deposition. Carbon 45(4):828–832
148. Wen Y, Kok MDR, Tafoya JPV, Sobrido ABJ, Bell E, Gostick JT, Herou S, Schlee P, Titirici M-M, Brett DJL, Shearing PR, Jervis R (2021) Electrospinning as a route to advanced carbon fibre materials for selected low-temperature electrochemical devices: a review. J Energ Che 59:492–529
149. Huang C, Soenen SJ, Rejman J, Lucas B, Braeckmans K, Demeester J, De Smedt SC (2011) Stimuli-responsive electrospun fibers and their applications. Chem Soc Rev 40(5):2417–2434
150. Ding B, Wang M, Wang X, Yu J, Sun G (2010) Electrospun nanomaterials for ultrasensitive sensors. Mater Today 13(11):16–27
151. Inagaki M, Yang Y, Kang F (2012) Carbon nanofibers prepared via electrospinning. Adv Mater 24(19):2547–2566
152. Zhang L, Aboagye A, Kelkar A, Lai C, Fong H (2014) A review: carbon nanofibers from electrospun polyacrylonitrile and their applications. J Mater Sci 9(2):463–480
153. Qing-qiang K, Mang-guo Y, Cheng-meng C, Yong-gang Y (2012) Preparation and characterization of graphene-reinforced polyacrylonitrile-based carbon nanofibers. New Carbon Mater 27(3):188
154. Zhang L, Hsieh Y-L (2009) Carbon nanofibers with nanoporosity and hollow channels from binary polyacrylonitrile systems. Eur Polym J 45(1):47–56
155. Kim C, Yang KS, Kojima M, Yoshida K, Kim YJ, Kim YA, Endo M (2006) Fabrication of electrospinning-derived carbon nanofiber webs for the anode material of lithium-ion secondary batteries. Adv Func Mater 16(18):2393–2397
156. Zussman E, Chen X, Ding W, Calabri L, Dikin DA, Quintana JP, Ruoff RS (2005) Mechanical and structural characterization of electrospun PAN-derived carbon nanofibers. Carbon 43(10):2175–2185
157. Hou H, Ge JJ, Zeng J, Li Q, Reneker DH, Greiner A, Cheng SZD (2005) Electrospun polyacrylonitrile nanofibers containing a high concentration of well-aligned multiwall carbon nanotubes. Chem Mater 17(5):967–973
158. Ko F, Gogotsi Y, Ali A, Naguib N, Ye H, Yang GL, Li C, Willis P (2003) Electrospinning of continuous carbon nanotube-filled nanofiber yarns. Adv Mater 15(14):1161–1165
159. Geim AK, Novoselov KS (2007) The rise of graphene. Nat Mater 6(3):183–191
160. Morozov SV, Novoselov KS, Katsnelson MI, Schedin F, Elias DC, Jaszczak JA, Geim AK (2008) Giant intrinsic carrier mobilities in graphene and its bilayer. Phys Rev Lett 100(1):016602
161. Ferrari AC, Bonaccorso F, Fal'ko V, Novoselov KS, Roche S, Bøggild P, Borini S, Koppens FHL, Palermo V, Pugno N, Garrido JA, Sordan R, Bianco A, Ballerini L, Prato M, Lidorikis E, Kivioja J, Marinelli C, Ryhänen T, Morpurgo A, Coleman JN, Nicolosi V, Colombo L, Fert A, Garcia-Hernandez M, Bachtold A, Schneider GF, Guinea F, Dekker C, Barbone M, Sun Z, Galiotis C, Grigorenko AN, Konstantatos G, Kis A, Katsnelson M, Vandersypen L, Loiseau A, Morandi V, Neumaier D, Treossi E, Pellegrini V, Polini M, Tredicucci A, Williams GM, Hee Hong B, Ahn J-H, Min Kim J, Zirath H, van Wees BJ, van der Zant H, Occhipinti L,

Di Matteo A, Kinloch IA, Seyller T, Quesnel E, Feng X, Teo K, Rupesinghe N, Hakonen P, Neil SRT, Tannock Q, Löfwander T, Kinaret J (2015) Science and technology roadmap for graphene, related two-dimensional crystals, and hybrid systems. Nanoscale 7(11):4598–4810
162. Kumar P, Yu S, Shahzad F, Hong SM, Kim Y-H, Koo CM (2016) Ultrahigh electrically and thermally conductive self-aligned graphene/polymer composites using large-area reduced graphene oxides. Carbon 101:120–128
163. Kumar P, Narayan Maiti U, Sikdar A, Kumar Das T, Kumar A, Sudarsan V (2019) Recent advances in polymer and polymer composites for electromagnetic interference shielding: review and future prospects. Polym Rev 59(4):687–738
164. Kumar P, Shahzad F, Hong SM, Koo CM (2016) A flexible sandwich graphene/silver nanowires/graphene thin film for high-performance electromagnetic interference shielding. RSC Advances 6(103):101283–101287
165. Kumar P, Kumar A, Cho KY, Das TK, Sudarsan V (2017) An asymmetric electrically conducting self-aligned graphene/polymer composite thin film for efficient electromagnetic interference shielding. AIP Advances 7(1):015103
166. Kumar P, Yadav MK, Panwar N, Kumar A, Singhal R (2019) Temperature dependent thermal conductivity of free-standing reduced graphene oxide/poly (vinylidene fluoride-co-hexafluoropropylene) composite thin film. Mater Res Express 6(11):115604
167. Bolotin KI, Sikes KJ, Jiang Z, Klima M, Fudenberg G, Hone J, Kim P, Stormer HL (2008) Ultrahigh electron mobility in suspended graphene. Solid State Commun 146(9):351–355
168. Soldano C, Mahmood A, Dujardin E (2010) Production, properties and potential of graphene. Carbon 48(8):2127–2150
169. Hernandez Y, Nicolosi V, Lotya M, Blighe FM, Sun ZY, De S, McGovern IT, Holland B, Byrne M, Gun'ko YK, Boland JJ, Niraj P, Duesberg G, Krishnamurthy S, Goodhue R, Hutchison J, Scardaci V, Ferrari AC, Coleman JN (2008) High-yield production of graphene by liquid-phase exfoliation of graphite. Nat Nanotechnol 3(9):563–568
170. Blake P, Brimicombe PD, Nair RR, Booth TJ, Jiang D, Schedin F, Ponomarenko LA, Morozov SV, Gleeson HF, Hill EW, Geim AK, Novoselov KS (2008) Graphene-based liquid crystal device. Nano Lett 8:1704–1708
171. Hernandez Y, Lotya M, Rickard D, Bergin SD, Coleman JN (2010) Measurement of multicomponent solubility parameters for graphene facilitates solvent discovery. Langmuir 26(5):3208–3213
172. Vallés C, Drummond C, Saadaoui H, Furtado CA, He M, Roubeau O, Ortolani L, Monthioux M, Pénicaud A (2008) Solutions of negatively charged graphene sheets and ribbons. J Am Chem Soc 130(47):15802–15804
173. Behabtu N, Lomeda JR, Green MJ, Higginbotham AL, Sinitskii A, Kosynkin DV, Tsentalovich D, Parra-Vasquez ANG, Schmidt J, Kesselman E, Cohen Y, Talmon Y, Tour JM, Pasquali M (2010) Spontaneous high-concentration dispersions and liquid crystals of graphene. Nat Nanotechnol 5(6):406–411
174. Lotya M, Hernandez Y, King PJ, Smith RJ, Nicolosi V, Karlsson LS, Blighe FM, De S, Wang ZM, McGovern IT, Duesberg GS, Coleman JN (2009) Liquid phase production of graphene by exfoliation of graphite in surfactant/water solutions. J Am Chem Soc 131(10):3611–3620
175. Lotya M, King P, Khan U, De S, Coleman JN (2010) Coleman, high-concentration, surfactant-stabilized graphene dispersions. ACS Nano 4(6):3155–3162
176. Parvez K, Wu Z-S, Li R, Liu X, Graf R, Feng X, Mìllen K (2014) Exfoliation of graphite into graphene in aqueous solutions of inorganic salts. J Am Chem Soc 136(16):6083–6091
177. Huang X, Qi X, Boey F, Zhang H (2012) Graphene-based composites. Chem Soc Rev 41(2):666–686
178. Low CTJ, Walsh FC, Chakrabarti MH, Hashim MA, Hussain MA (2013) Electrochemical approaches to the production of graphene flakes and their potential applications. Carbon 54:1–21
179. Su C-Y, Lu A-Y, Xu Y, Chen F-R, Khlobystov AN, Li L-J (2011) High-quality thin graphene films from fast electrochemical exfoliation. ACS Nano 5(3):2332–2339

180. Alanyalıoğlu M, Segura JJ, Oró-Solè J, Casañ-Pastor N (2012) The synthesis of graphene sheets with controlled thickness and order using surfactant-assisted electrochemical processes. Carbon 50(1):142–152
181. Wang J, Manga KK, Bao Q, Loh KP (2011) High-yield synthesis of few-layer graphene flakes through electrochemical expansion of graphite in propylene carbonate electrolyte. J Am Chem Soc 133(23):8888–8891
182. Ambrosi A, Pumera M (2015) Electrochemically exfoliated graphene and graphene oxide for energy storage and electrochemistry applications. Chem: Euro J 22(1):153–159
183. Brodie BC (2009) On the atomic weight of graphite. https://nbn-resolving.org/urn:nbn:de:hebis:30-1133136
184. Staudenmaier L (1898) Verfahren zur Darstellung der Graphitsäure. Ber Dtsch Chem Ges 31(2):1481–1487
185. Dreyer DR, Ruoff RS, Bielawski CW (2010) From conception to realization: an historial account of graphene and some perspectives for its future. Angew Chem Int Ed 49(49):9336–9344
186. Zhu Y, Murali S, Cai W, Li X, Suk JW, Potts JR, Ruoff RS (2010) Graphene and graphene oxide: synthesis, properties, and applications. Adv Mater 22(35):3906–3924
187. Stankovich S, Dikin DA, Dommett GHB, Kolhaas KM, Zimney EJ, Stach EA, Piner RD, Nguyen ST, Ruoff RS (2006) Graphene-based composite materials. Nature 442(7100):282–286
188. Kumar P, Shahzad F, Yu S, Hong SM, Kim Y-H, Koo CM (2015) Large-area reduced graphene oxide thin film with excellent thermal conductivity and electromagnetic interference shielding effectiveness. Carbon 94:494–500
189. Kumar P, Maiti UN, Lee KE, Kim SO (2014) Rheological properties of graphene oxide liquid crystal. Carbon 80:453–461
190. Cho KY, Yeom YS, Seo HY, Kumar P, Lee AS, Baek K-Y, Yoon HG (2017) Molybdenum-doped PdPt@Pt core–shell octahedra supported by ionic block copolymer-functionalized graphene as a highly active and durable oxygen reduction electrocatalyst. ACS Appl Mater Interfaces 9(2):1524–1535
191. Cho KY, Yeom YS, Seo HY, Kumar P, Lee AS, Baek K-Y, Yoon HG (2015) Ionic block copolymer doped reduced graphene oxide supports with ultra-fine Pd nanoparticles: strategic realization of ultra-accelerated nanocatalysis. J Mater Chem A 3(41):20471–20476
192. Cho KY, Seo HY, Yeom YS, Kumar P, Lee AS, Baek K-Y, Yoon HG (2016) Stable 2D-structured supports incorporating ionic block copolymer-wrapped carbon nanotubes with graphene oxide toward compact decoration of metal nanoparticles and high-performance nano-catalysis. Carbon 105:340–352
193. Dimiev AM, Tour JM (2014) Mechanism of graphene oxide formation. ACS Nano 8(3):3060–3068
194. Kim JE, Han TH, Lee SH, Kim JY, Ahn CW, Yun JM, Kim SO (2011) Graphene oxide liquid crystals. Angew Chem Int Ed 50(13):3043–3047
195. Ang PK, Wang S, Bao Q, Thong JTL, Loh KP (2009) High-throughput synthesis of graphene by intercalation−exfoliation of graphite oxide and study of ionic screening in graphene transistor. ACS Nano 3(11):3587–3594
196. Eigler S, Enzelberger-Heim M, Grimm S, Hofmann P, Kroener W, Geworski A, Dotzer C, Röckert M, Xiao J, Papp C, Lytken O, Steinrück H-P, Müller P, Hirsch A (2013) Wet chemical synthesis of graphene. Adv Mater 25(26):3583–3587
197. Peng L, Xu Z, Liu Z, Wei Y, Sun H, Li Z, Zhao X, Gao C (2015) An iron-based green approach to 1-h production of single-layer graphene oxide. Nat Commun 6:5716
198. Schniepp HC, Li J-L, McAllister MJ, Sai H, Herrera-Alonso M, Adamson DH, Prud'homme RK, Car R, Saville DA, Aksay IA (2006) Functionalized single graphene sheets derived from splitting graphite oxide. J Phys Chem B 110(17):8535–8539
199. McAllister MJ, Li JL, Adamson DH, Schniepp HC, Abdala AA, Liu J, Herrera-Alonso M, Milius DL, Car R, Prud'homme RK, Aksay IA (2007) Single sheet functionalized graphene by oxidation and thermal expansion of graphite. Chem Mater 19(18):4396–4404

200. Xin G, Sun H, Hu T, Fard HR, Sun X, Koratkar N, Borca-Tasciuc T, Lian J (2014) Large-area freestanding graphene paper for superior thermal management. Adv Mater 26(26):4521–4526
201. Kotov NA, Dékány I, Fendler JH (1996) Ultrathin graphite oxide–polyelectrolyte composites prepared by self-assembly: transition between conductive and non-conductive states. Adv Mater 8(8):637–641
202. Ambrosi A, Bonanni A, Sofer Z, Cross JS, Pumera M (2011) Electrochemistry at chemically modified graphenes. Chem: Euro J 17(38):10763–10770
203. Jin AS, Yanwu Z, Hwa LS, Meryl DS, Tryggvi E, Sungjin P, Aruna V, Jinho A, Rodney RS (2010) J Phys Chem Lett 1:1259
204. Ambrosi A, Pumera M (2013) Precise tuning of surface composition and electron-transfer properties of graphene oxide films through electroreduction. Chem Euro J 19(15):4748–4753
205. Hofmann U, König E (1937) Untersuchungen über Graphitoxyd. Zeitschrift für anorganische und allgemeine Chemie 234(4):311–336
206. Becerril HA, Mao J, Liu Z, Stoltenberg RM, Bao Z, Chen Y (2008) Evaluation of solution-processed reduced graphene oxide films as transparent conductors. ACS Nano 2(3):463–470
207. Park S, An J, Potts JR, Velamakanni A, Murali S, Ruoff RS (2011) Hydrazine-reduction of graphite- and graphene oxide. Carbon 49(9):3019–3023
208. Shin H-J, Sim KK, Benayad A, Yoon S-M, Park HK, Jung I-S, Jin MH, Jeong H-K, Kim JM, Choi J-Y, Lee YH (2009) Efficient reduction of graphite oxide by sodium borohydride and its effect on electrical conductance. Adv Func Mater 19(12):1987–1992
209. Pei S, Zhao J, Du J, Ren W, Cheng H-M (2010) Direct reduction of graphene oxide films into highly conductive and flexible graphene films by hydrohalic acids. Carbon 48(15):4466–4474
210. Gao W, Alemany LB, Ci LJ, Ajayan PM (2009) New insights into the structure and reduction of graphite oxide. Nat Chem 1(5):403–408
211. Wang G, Yang J, Park J, Gou X, Wang B, Liu H, Yao J (2008) Facile synthesis and characterization of graphene nanosheets. J Phys Chem C 112(22):8192–8195
212. Thakur S, Karak N (2012) Green reduction of graphene oxide by aqueous phytoextracts. Carbon 50(14):5331–5339
213. Akhavan O, Ghaderi E (2012) Escherichia coli bacteria reduce graphene oxide to bactericidal graphene in a self-limiting manner. Carbon 50(5):1853–1860
214. Cote LJ, Cruz-Silva R, Huang JX (2009) Flash reduction and patterning of graphite oxide and its polymer composite. J Am Chem Soc 131(31):11027–11032
215. Ji T, Hua Y, Sun M, Ma N (2013) The mechanism of the reaction of graphite oxide to reduced graphene oxide under ultraviolet irradiation. Carbon 54:412–418
216. Strong V, Dubin S, El-Kady MF, Lech A, Wang Y, Weiller BH, Kaner RB (2012) Patterning and electronic tuning of laser scribed graphene for flexible all-carbon devices. ACS Nano 6(2):1395–1403
217. Jiao L, Zhang L, Wang X, Diankov G, Dai H (2009) Narrow graphene nanoribbons from carbon nanotubes. Nature 458(7240):877–880
218. Higginbotham A, Kosynkin D, Sinitskii A, Sun Z, Tour JM (2010) Lower-defect graphene oxide nanoribbons from multiwalled carbon nanotubes. ACS Nano 4(4):2059–2069
219. Kosynkin DV, Higginbotham AL, Sinitskii A, Lomeda JR, Dimiev A, Price BK, Tour JM (2009) Longitudinal unzipping of carbon nanotubes to form graphene nanoribbons. Nature 458(7240):872–876
220. Wei D, Liu Y (2010) Controllable synthesis of graphene and its applications. Adv Mater 22:3225–3241
221. J. Li, S. Ye, T. Li, X. Li, X. Yang, S. Ding, Preparation of Graphene Nanoribbons (GNRs) as an Electronic Component with the Multi-walled Carbon Nanotubes (MWCNTs), Procedia Engineering 102 (2015):492–498
222. Xiao B, Li X, Li X, Wang B, Langford C, Li R, Sun X (2014) Graphene nanoribbons derived from the unzipping of carbon nanotubes: controlled synthesis and superior lithium storage performance. J Phys Chem C 118(2):881–890
223. Lim J, Maiti UN, Kim N-Y, Narayan R, Lee WJ, Choi DS, Oh Y, Lee JM, Lee GY, Kang SH, Kim H, Kim Y-H, Kim SO (2016) Dopant-specific unzipping of carbon nanotubes for intact crystalline graphene nanostructures. Nat Commun 7(1):10364

224. Elías AL, Botello-Méndez AR, Meneses-Rodríguez D, Jehová González V, Ramírez-González D, Ci L, Muñoz-Sandoval E, Ajayan PM, Terrones H, Terrones M (2009) Longitudinal cutting of pure and doped carbon nanotubes to form graphitic nanoribbons using metal clusters as nanoscalpels. Nano Lett 10(2):366–372
225. Li Y-S, Liao J-L, Wang S-Y, Chiang W-H (2016) Intercalation-assisted longitudinal unzipping of carbon nanotubes for green and scalable synthesis of graphene nanoribbons. Sci Rep 6(1):22755
226. Cano-Márquez A, Rodríguez-Macías F, Campos-Delgado J, Espinosa-González C, Tristán-López F, Ramírez-González D, Cullen D, Smith D, Terrones M, Vega-Cantú Y (2009) Ex-Mwnts: graphene sheets and ribbons produced by lithium intercalation and exfoliation of carbon nanotubes. Nano Letter 9:1527–1533
227. Kim WS, Moon SY, Bang SY, Choi BG, Ham H, Sekino T, Shim KB (2009) Fabrication of graphene layers from multiwalled carbon nanotubes using high dc pulse. Appl Phys Lett 95(8):083103
228. Wu JS, Pisula W, Mullen K (2007) Graphenes as potential material for electronics. Chem Rev 107:718–747
229. Proceedings of the Chemical Society (May) (1958) 125–156
230. Simpson CD, Brand JD, Berresheim AJ, Przybilla L, Rader HJ, Mullen K (2002) Synthesis of a giant 222 carbon graphite sheet. Chem Eur J 8(6):1424–1429
231. Eizenberg M, Blakely JM (1979) Carbon monolayer phase condensation on Ni(111). Surf Sci 82(1):228–236
232. Aizawa T, Souda R, Otani S, Ishizawa Y, Oshima C (1990) Anomalous bond of monolayer graphite on transition-metal carbide surfaces. Phys Rev Lett 64(7):768–771
233. Cui Y, Fu Q, Bao X (2010) Dynamic observation of layer-by-layer growth and removal of graphene on Ru(0001). Phys Chem Chem Phys 12(19):5053–5057
234. Liu M, Zhang Y, Chen Y, Gao Y, Gao T, Ma D, Ji Q, Zhang Y, Li C, Liu Z (2012) Thinning segregated graphene layers on high carbon solubility substrates of rhodium foils by tuning the quenching process. ACS Nano 6(12):10581–10589
235. Sutter P, Sadowski JT, Sutter E (2009) Graphene on Pt(111): growth and substrate interaction. Phys Rev B 80(24):245411
236. Nie S, Walter AL, Bartelt NC, Starodub E, Bostwick A, Rotenberg E, McCarty KF (2011) Growth from below: graphene bilayers on Ir(111). ACS Nano 5(3):2298–2306
237. Li X, Cai W, Colombo L, Ruoff RS (2009) Evolution of graphene growth on Ni and Cu by carbon isotope labeling. Nano Lett 9(12):4268–4272
238. Kim R-H, Bae M-H, Kim DG, Cheng H, Kim BH, Kim D-H, Li M, Wu J, Du F, Kim H-S, Kim S, Estrada D, Hong SW, Huang Y, Pop E, Rogers JA (2011) Stretchable, transparent graphene interconnects for arrays of microscale inorganic light emitting diodes on rubber substrates. Nano Lett 11(9):3881–3886
239. Reina A, Jia X, Ho J, Nezich D, Son H, Bulovic V, Dresselhaus MS, Kong J (2009) Large area, few-layer graphene films on arbitrary substrates by chemical vapor deposition. Nano Lett 9(1):30–35
240. Sun Z, Yan Z, Yao J, Beitler E, Zhu Y, Tour JM (2010) Growth of graphene from solid carbon sources. Nature 468(7323):549–552
241. Yu Q, Lian J, Siriponglert S, Li H, Chen YP, Pei S-S (2008) Graphene segregated on Ni surfaces and transferred to insulators. Appl Phys Lett 93(11):113103
242. Li X, Cai W, An J, Kim S, Nah J, Yang D, Piner R, Velamakanni A, Jung I, Tutuc E, Banerjee SK, Colombo L, Ruoff RS (2009) Large-area synthesis of high-quality and uniform graphene films on copper foils. Science 324(5932):1312–1314
243. Arco LGD, Zhang Y, Kumar A, Zhou C (2009) Synthesis, transfer, and devices of single- and few-layer graphene by chemical vapor deposition. IEEE Trans Nanotechnol 8(2):135–138
244. Kim KS, Zhao Y, Jang H, Lee SY, Kim JM, Kim KS, Ahn J-H, Kim P, Choi J-Y, Hong BH (2009) Large-scale pattern growth of graphene films for stretchable transparent electrodes. Nature 457(7230):706–710

245. Li X, Magnuson CW, Venugopal A, Tromp RM, Hannon JB, Vogel EM, Colombo L, Ruoff RS (2011) Large-area graphene single crystals grown by low-pressure chemical vapor deposition of methane on copper. J Am Chem Soc 133(9):2816–2819
246. Gong Y, Zhang X, Liu G, Wu L, Geng X, Long M, Cao X, Guo Y, Li W, Xu J, Sun M, Lu L, Liu L (2012) Layer-controlled and wafer-scale synthesis of uniform and high-quality graphene films on a polycrystalline nickel catalyst. Adv Func Mater 22(15):3153–3159
247. Zhang Y, Zhang L, Zhou C (2013) Review of chemical vapor deposition of graphene and related applications. Accounts Chem Res 46(10):2329–2339
248. Kang J, Shin D, Bae S, Hong B (2012) Graphene transfer: key for applications. Nanoscale 4(18):5527–5537
249. Liang X, Sperling BA, Calizo I, Cheng G, Hacker CA, Zhang Q, Obeng Y, Yan K, Peng H, Li Q, Zhu X, Yuan H, Walker ARH, Liu Z, Peng L-M, Richter CA (2011) Toward clean and crackless transfer of graphene. ACS Nano 5(11):9144–9153
250. Li X, Zhu Y, Cai W, Borysiak M, Han B, Chen D, Piner R, Colombo L, Ruoff RS (2009) Transfer of large-area graphene films for high-performance transparent conductive electrodes. Nano Lett 9(12):4359–4363
251. Martins LG, Song Y, Zeng T, Dresselhaus MS, Kong J, Araujo PT (2013) Direct transfer of graphene onto flexible substrates. Proc Natl Acad Sci 110(44):17762–7
252. Hu FM, Ma TX, Lin HQ, Gubernatis JE (2011) Magnetic impurities in graphene. Phys Rev B 84(7):075414
253. Krasheninnikov AV, Nieminen RM (2011) Attractive interaction between transition-metal atom impurities and vacancies in graphene: a first-principles study. Theoret Chem Acc 129(3):625–630
254. Alemán B, Regan W, Aloni S, Altoe V, Alem N, Girit C, Geng BS, Maserati L, Crommie M, Wang F, Zettl A (2010) Transfer-free batch fabrication of large-area suspended graphene membranes. ACS Nano 4(8):4762–4768
255. Ambrosi A, Pumera M (2014) The CVD graphene transfer procedure introduces metallic impurities which alter the graphene electrochemical properties. Nanoscale 6(1):472–476
256. Gorantla S, Bachmatiuk A, Hwang J, Alsalman HA, Kwak JY, Seyller T, Eckert J, Spencer MG, Rummeli MH (2014) A universal transfer route for graphene. Nanoscale 6(2):889–896
257. Gao L, Ni G-X, Liu Y, Liu B, Castro Neto AH, Loh KP (2014) Face-to-face transfer of wafer-scale graphene films. Nature 505(7482):190–194
258. Jacob MV, Rawat RS, Ouyang B, Bazaka K, Kumar DS, Taguchi D, Iwamoto M, Neupane R, Varghese OK (2015) Catalyst-free plasma enhanced growth of graphene from sustainable sources. Nano Lett 15(9):5702–5708
259. Kar R, Patel NN, Chand N, Shilpa RK, Dusane RO, Patil DS, Sinha S (2016) Detailed investigation on the mechanism of co-deposition of different carbon nanostructures by microwave plasma CVD. Carbon 106:233–242
260. Emtsev KV, Bostwick A, Horn K, Jobst J, Kellogg GL, Ley L, McChesney JL, Ohta T, Reshanov SA, Roehrl J, Rotenberg E, Schmid AK, Waldmann D, Weber HB, Seyller T (2009) Towards wafer-size graphene layers by atmospheric pressure graphitization of silicon carbide. Nat Mater 8(3):203–7
261. Tromp RM, Hannon JB (2009) Thermodynamics and kinetics of graphene growth on SiC(0001). Phys Rev Lett 102(10):106104
262. Mishra N, Boeck J, Motta N, Iacopi F (2016) Graphene growth on silicon carbide: A review. Phys Status Solidi A 213(9):2277–2289
263. Hupalo M, Conrad EH, Tringides MC (2009) Growth mechanism for epitaxial graphene on vicinal $6H\text{-SiC}(0001)$ surfaces: A scanning tunneling microscopy study. Phys Rev B 80(4):041401
264. Moreau E, Ferrer FJ, Vignaud D, Godey S, Wallart X (2010) Graphene growth by molecular beam epitaxy using a solid carbon source. Phys Status Solidi A 207(2):300–303
265. Hu M, Yao Z, Wang X (2017) Graphene-based nanomaterials for catalysis. Ind Eng Chem Res 56(13):3477–3502

266. Ambrosi A, Chua CK, Bonanni A, Pumera M (2014) Electrochemistry of graphene and related materials. Chem Rev 114(14):7150–7188
267. Syama S, Mohanan PV (2019) Comprehensive application of graphene: emphasis on biomedical concerns. Nano-Micro Lett 11(1):6